CHAPTER 8

FLUID CHEMISTRY

8.1 Introduction

This chapter investigates the character and origins of fluids responsible for mineralization and alteration at PBH and Kerikil using available fluid inclusion data (from Simmons and Browne, 1990) and new stable isotope geochemistry. The aim of this study was to characterize the environment of deposition and potential source fluids for both metals and gangue minerals. Variations in the temperature, salinity and isotopic character of the fluids for different infill stages and alteration facies at PBH and Kerikil are discussed.

8.2 Fluid inclusion data review

Fluid inclusion data were reported by Simmons and Browne (1990) for samples from the Mt Muro deposits. These data include more than 300 heating and freezing measurements on 25 samples from Kerikil, and 31 measurements on 5 samples from PBH (Table 8.1). As noted by Simmons (1988), fluid inclusions at Mt Muro and Luit (PBH), in particular, are difficult to measure due to the fine-grained nature of the quartz and evidence for necking in many inclusions. Additional measurements were not carried out in this study. Attempts to measure fluid inclusions within the paragenetic stages not included in the Simmons and Browne (1990) study were unsuccessful due to the very fine-grained nature of quartz within the ore stages and poor preservation of inclusions due to necking. However, in this section, the data from Simmons and Browne (1990) are summarized (Table 8.1) and reviewed in the context of the revised paragenetic sequence for Kerikil and PBH.

8.2.1 PBH fluid inclusions

Simmons and Browne (1990) studied only 5 samples from PBH that were taken from coarse-grained, late vein stages (equivalent to stages 4 and 5 in this study). Fluid

Table 8.1 PBH and Kerikil fluid inclusion microthermometry (Simmons and Browne, 1990)

Fluid homogenization temperatures for PBH and Kerikil as maximum, minimum and mean values. Also shown are melting temperatures and equivalent fluid salinity values. Paleodepth below water table estimates are determined from fluid-inclusion boiling evidence (coexisting vapor- and liquid-rich inclusions) and pressure corrections to homogenizarion temperatures. Pressure-depth estimates assume a salinity of 2 wt % NaCl equiv..

			T_h (° C)	T_h (° C)	T_h (° C)	Salinity		Pressure estimate from boiling properties		Depth below water table (m)
Deposit	Vein stage	n	min	max	mean	T_m (° C)	NaCl wt. % equiv.	T_h (° C)	P (bars)	
Kerikil	all	482	207	253	228	- 2.5 to - 1.48	< 4.1	207 - 253	19 - 46	225 - 400
PBH	all	51	238	261	252	1.1 to - 1.48	< 3.2	238	33	> 400

inclusion homogenization temperatures for these samples range from 238 to 262° C with salinities of less than 3.2 wt % NaCl equiv. (Table 8.1). Only one sample (sampled at 120 RL) contained evidence for boiling (i.e., coexisting liquid- and vapor-rich inclusions; Simmons and Browne, 1990). Pressure-depth estimates for this sample equate to approximately 33 bars and a corresponding depth below the paleo-water table of approximately 400 m. Higher homogenization temperatures from liquid-rich inclusions suggest depths below the water table of greater than 500 m.

8.2.2 Kerikil fluid inclusions

Most of the fluid inclusion data reported by Simmons and Browne (1990) for Kerikil were from samples from stages 3 and 4 of their paragenesis (equivalent to stages 7 and 8 in this study). Earlier stages were unsuitable for fluid inclusion analysis. Most of the fluid inclusions studied were primary, liquid-rich inclusions in sphalerite and quartz that yielded homogenization temperatures ranging from 207 to 253°C. Ice melting temperatures for these samples range from - 0.2 to 2.5°C, equivalent to fluids containing less than 4.1 wt% NaCl equiv. (Table 8.1). Simmons and Browne (1990) state that these salinities could be as low as 1.5 wt % NaCl equiv. if there was appreciable dissolved CO_2 in the inclusions.

Many Kerikil samples contain coexisting liquid- and vapor-rich inclusions (Simmons and Browne, 1990), providing good evidence for boiling at the time of mineral precipitation (Roedder, 1984). Evidence for boiling allows the estimation of fluid pressure and paleo-depth of formation relative to the water table (e.g., Haas, 1971). Homogenization temperatures of 207 to 253°C in the Kerikil samples correspond to fluid pressures between 19 and 46 bars (Haas, 1971) for a fluid containing 2.0 wt % NaCl equiv. Assuming hydrostatic conditions, the water table was at least 225 to 400 m above the present day erosion surface (Simmons and Browne, 1990).

Further observations by Simmons and Browne (1990) are particularly relevant to the model proposed in this study for the sealing and brecciation of the Kerikil deposit (Chapter 5). In two samples from stage 7, successive generations of quartz display an increase in the proportion of vapor-rich to liquid-rich inclusions with time and the youngest generation of quartz contains only vapor-rich inclusions. This was interpreted to represent the development of a steam-dominated zone beneath a locally sealed conduit, immediately prior to hydrothermal eruption, which could have been initiated by tectonic fracturing (Simmons and Browne, 1990). Alternatively, this trend in fluid inclusion types may also be related to excess steam production due to magma emplacement (possibly as a dike) into the wallrocks adjacent to the active hydrothermal system.

8.2.3 Implications of fluid inclusion data

Data from Simmons and Browne (1990) indicate that the PBH deposit formed at greater depth and higher temperatures than Kerikil. This is at odds with the model of Corbett and Leach (1998) who suggest that the carbonate-base metal-gold deposits of the Southwest Pacific, which have very similar characteristics to Kerikil, represent a deeper and hotter style of epithermal gold mineralization than quartz-adularia-sericite deposits, which are similar to PBH.

In general, fluids that formed the PBH and Kerikil deposits were dilute and their compositions are consistent with a shallow meteoric origin, rather than a deep saline source. Fluid inclusions also provide textural evidence for boiling at PBH and Kerikil and suggest over-pressurization due to self-sealing processes at Kerikil (Simmons and Browne, 1990).

8.3 Stable isotope geochemistry

Stable isotope analyses can be used to determine the source and nature of different mineral components, the physiochemical conditions of mineral deposition, and/or can provide a measure of fluid-rock interaction. Stable isotope techniques had not been applied to the Mt Muro deposits prior to this study, and the results are used here to provide further constraints for the ore genesis model.

Stable isotope data were generated for sulfides ($\delta^{34}S$), carbonates ($\delta^{13}C$ and $\delta^{18}O$), quartz separates ($\delta^{18}O$), and whole rock samples ($\delta^{18}O$) from both PBH and Kerikil. Pyrite was the main sulfide analyzed since it is ubiquitous across infill stages and alteration facies, and is sufficiently coarse-grained that it could be extracted manually for conventional analysis. Carbonate samples include both calcite and rhodochrosite that were selected from veins and breccia zones across multiple paragenetic stages. Whole rock samples were selected from each alteration facies and quartz mineral separates were extracted manually from each infill stage.

8.3.1 Analytical methods

Sulfur isotope analyses were carried out on sulfide mineral separates drilled from samples of coarse-grained sulfides using conventional methods (after Robinson and Kukasabe, 1975). All sulfur isotope ratios were measured on a VG Micromass 602D mass spectrometer at the Central Science Laboratory, University of Tasmania. Internal standards were run with an SO_2 reference gas and calibrated against international standards IAEA NZ1 and NBS 123. Results are expressed in standard $\delta^{34}S$ per mil (‰) notation, relative to the Canyon Diablo Troilite (CDT). Analytical uncertainty is ± 0.2 per mil.

Carbon and oxygen isotope data for calcite and rhodochrosite were measured at the Central Science Laboratory, University of Tasmania, according to the method of McCrea (1950). Carbonate was seperated from hand samples using a fine diamond drill. All samples were reacted with phosphoric acid at 25° C for 24 hours and analyzed using a Finigan Isogas 2000 mas spectrometer. Carbon results are expressed in standard $\delta^{13}C$ per mil (‰) notation relative to the Peedee Formation Belemnite (PDB). Oxygen data are expressed in standard $\delta^{18}O$ per mil (‰) relative to standard mean ocean water (SMOW).

The oxygen isotope composition of quartz mineral seperates and whole rock powders were analyzed at the University of Arizona, U.S.A. according to the methods of Clayton and Mayeda (1963). Quartz was drilled from hand samples using a fine dentist drill and hand-picked from crushed samples. Possible contamination of hand-picked samples was reduced by microscopic screening. Internal quartz standards, which are calibrated to NBDS-28, were run every 10 to 20 analyses. Repeated analyses of standards yielded a two sigma error of ± 0.15 per mil. Oxygen results are expressed in standard $\delta^{18}O$ per mil (‰) relative to standard mean ocean water (SMOW).

8.3.2 Sulfur isotope results

A total of 14 sulfur isotope analyses were completed on 13 pyrite samples and 1 sphalerite sample from veins and alteration facies at PBH and Kerikil. Results are summarized in Table 8.2 and Figure 8.1. Full details are provided in Appendix 6.

8.3.3 Sulfur isotope composition of sulfide

$\delta^{34}S_{sulfide}$ values for the two deposits range from -5.2 to +3.8‰ with a mean of 0.7‰. Mean $\delta^{34}S_{sulfide}$ values for Kerikil (1.8‰) are slightly higher than those for PBH (0.2‰). There is more variation in $\delta^{34}S$ values for the PBH sulfides compared to Kerikil, although this may be attributed, at least in part, to the larger dataset for PBH. Data for the

Table 8.2 PBH and Kerikil $\delta^{34}S$ values

Summary of sulfide $\delta^{34}S$ data for $\delta^{34}S$ for PBH and Kerikil as maximum, minimum and mean values.

Deposit	Sample Selection	n	$\delta^{34}S$ ‰ (CDT) Minimum	$\delta^{34}S$ ‰ (CDT) Maximum	$\delta^{34}S$ ‰ (CDT) Mean	$\delta^{34}S$ ‰ (CDT) Standard Deviation
All		14	-5.1	3.8	0.7	± 2.2
PBH	all	10	-5.1	3.1	0.2	± 2.6
	infill stage	2	-0.5	2.0	0.8	± 1.8
	alteration facies	8	-5.1	3.1	0.0	± 0.4
Kerikil	all	4	0.3	3.8	1.8	± 1.5
	infill stage	3	0.3	3.8	1.8	± 1.8
	alteration facies	1	1.8	1.8	1.8	-

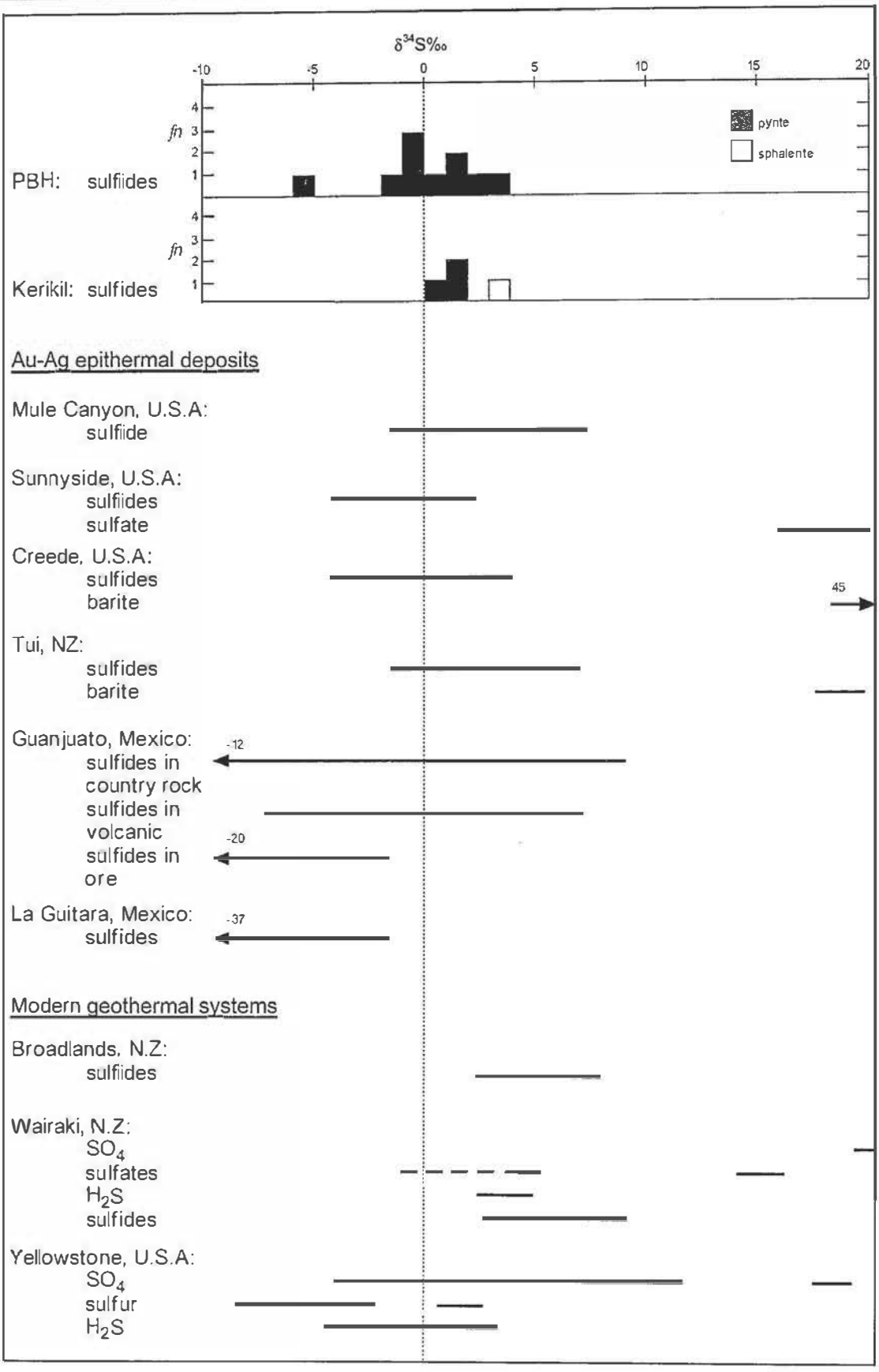

Figure 8.1 PBH and Kerikil $\delta^{34}S$ values for sulfides compared with selected ancient epithermal and modern geothermal systems

$\delta^{34}S$ data for pynte and sphalente from PBH and Kenkil (as lustrogram). Also shown are ranges for $\delta^{34}S$ values from selected Au-Aglow sulfidation epithermal deposits and modern geothermal systems (summarized from Field and Fifarak, 1985; Campubri et al., 2001, John et al, 2003)

one Kerikil sphalerite sample is comparable to that of pyrite (Fig. 8.1). A comparison of $\delta^{34}S$ values to RL (elevation) or spatial distribution did not identify any obvious trends.

In general, $\delta^{34}S$ values determined for the PBH and Kerikil samples are similar to those for other low sulfidation Au-Ag epithermal deposits and modern geothermal systems and are consistent with a reduced sulfur source (Fig. 8.1). The near-zero $\delta^{34}S$ values in the two deposits indicate the sulfur was derived from a magmatic sulfur source (e.g., Ohmoto and Rye, 1979; Field and Fiferak, 1984).

8.3.4 Carbon and oxygen isotope results

A total of 18 combined carbon and oxygen isotope analyses were completed on eleven rhodochrosite and seven calcite samples from PBH and Kerikil. The samples were selected across 4 carbonate vein and breccia infill stages. Results are summarized in Table 8.3 and Figure 8.2. Full details are provided in Appendix 7.

8.3.5 Carbon and oxygen isotope composition of carbonate

Samples from PBH were all selected from stage 6 carbonate infill, represented by both calcite and rhodochrosite. $\delta^{13}C$ results for these samples range from -11.1 to -4.7‰ with a mean value of -7.3 ‰, and $\delta^{18}O$ values range from 5.5 to 15.0‰ with a mean of 10.6 ‰ (Table 8.3 and Fig. 8.2). Kerikil carbonate samples consist entirely of rhodochorosite from infill stages 5, 6 and 7. These samples have $\delta^{13}C$ values in the range of -14.2 to -6.0‰ with a mean of -10.9 ‰. $\delta^{18}O$ values are from 12.6 to 19.6‰ with a mean of 16.1‰ (Table 8.3 and Fig. 8.2).

In general, $\delta^{13}C$ data for carbonate from infill stage 6 at PBH and stage 5 at Kerikil are comparable to values for magmatic carbon (-5 to -10‰; Barnes et al., 1978) and overlap with carbonate data from modern geothermal systems (Fig 8.2 and 8.3; Barnes et al., 1978). Later carbonate infill stages at Kerikil have lower $\delta^{13}C$ values, however, ranging down to -14‰. This change is accompanied by an increase in $\delta^{18}O$ values, to a maximum of nearly 20‰ in stage 6 carbonate. $\delta^{18}O$ data from PBH is similarly variable, although with lower overall values ranging from approximately 5 to 16‰ (Fig. 8.3).

Trends in isotope data for the carbonates in the two deposits suggest variations in depositional processes. The large range of $\delta^{18}O$ values for the PBH carbonates, compared

Table 8.3 PBH and Kerikil C-O isotope data

Maximum, minimum and mean $\delta^{13}C$ and $\delta^{18}O$ data for calcite and rhodochrosite infill stages from PBH and Kerikil.

Deposit	Sample Selection	n	δ^{13} C ‰ (PBD) Minimum	δ^{13} C ‰ (PBD) Maximum	δ^{13}C ‰ (PBD) Mean	δ^{13}C ‰ (PBD) Standard Deviation	δ^{18}O ‰ (SMOW) Minimum	δ^{18}O ‰ (SMOW) Maximum	δ^{18}O ‰ (SMOW) Mean	δ^{18}O ‰ (SMOW) Standard Deviation
All		**18**	**-14.2**	**-4.7**	**-9.0**	**± 3.0**	**5.5**	**19.6**	**13.8**	**± 4.0**
	all calcite infill stages	7	-10.2	-4.7	-6.9	± 1.89	5.5	15.0	10.6	± 3.9
	all rhodochrosite infill stages	11	-14.2	-6.0	-10.9	± 2.5	12.6	19.6	16.1	± 2.8
PBH	all	9	**-11.1**	**-4.7**	**-7.3**	**± 2.2**	**5.5**	**16.0**	**11.5**	**± 3.9**
	stage 6, calcite infill	7	-10.2	-4.7	-6.9	± 1.89	5.5	15.0	10.6	± 3.9
	Stage 6, rhodochrosite infill	2	-11.1	-5.8	-8.5	± 3.8	13.2	16.0	14.6	± 2.0
Kerikil	all	9	**-14.2**	**-6.0**	**-10.9**	**± 2.6**	**12.6**	**19.6**	**16.1**	**± 2.8**
	stage 5, rhodochrosite infill	4	-10.9	6.0	-8.7	± 2.0	12.6	14.5	13.4	± 0.9
	stage 6, rhodochrosite infill	2	-14.2	-12.2	-13.2	± 1.4	18.6	19.6	19.2	± 0.5
	stage 7, rhodochrosite infill	3	-13.1	-11.9	-12.4	± 0.7	16.0	18.9	17.7	± 1.5

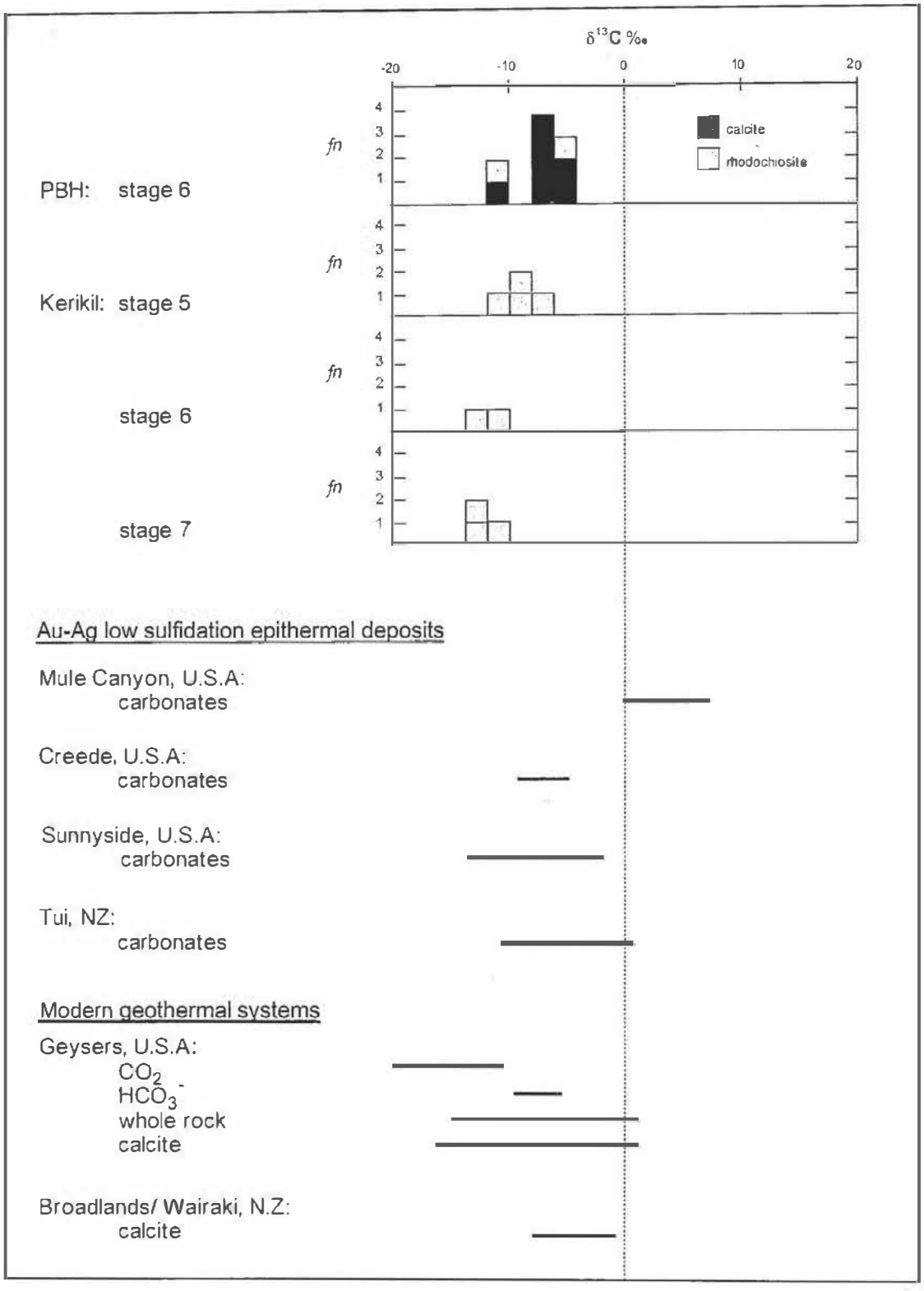

Figure 8.2 PBH and Kerikil $\delta^{13}C$ data for carbonate infill stages compared with selected ancient and modern geothermal systems

$\delta^{13}C$ values for calcite and rhodochrosite at PBH and Kerikil (as histograms). Also shown are ranges of $\delta^{13}C$ values from from selected Au-Ag low sulfidation epithermal deposits and modern geothermal systems (summarized from Field and Fiferak, 1985; John et al., 2003).

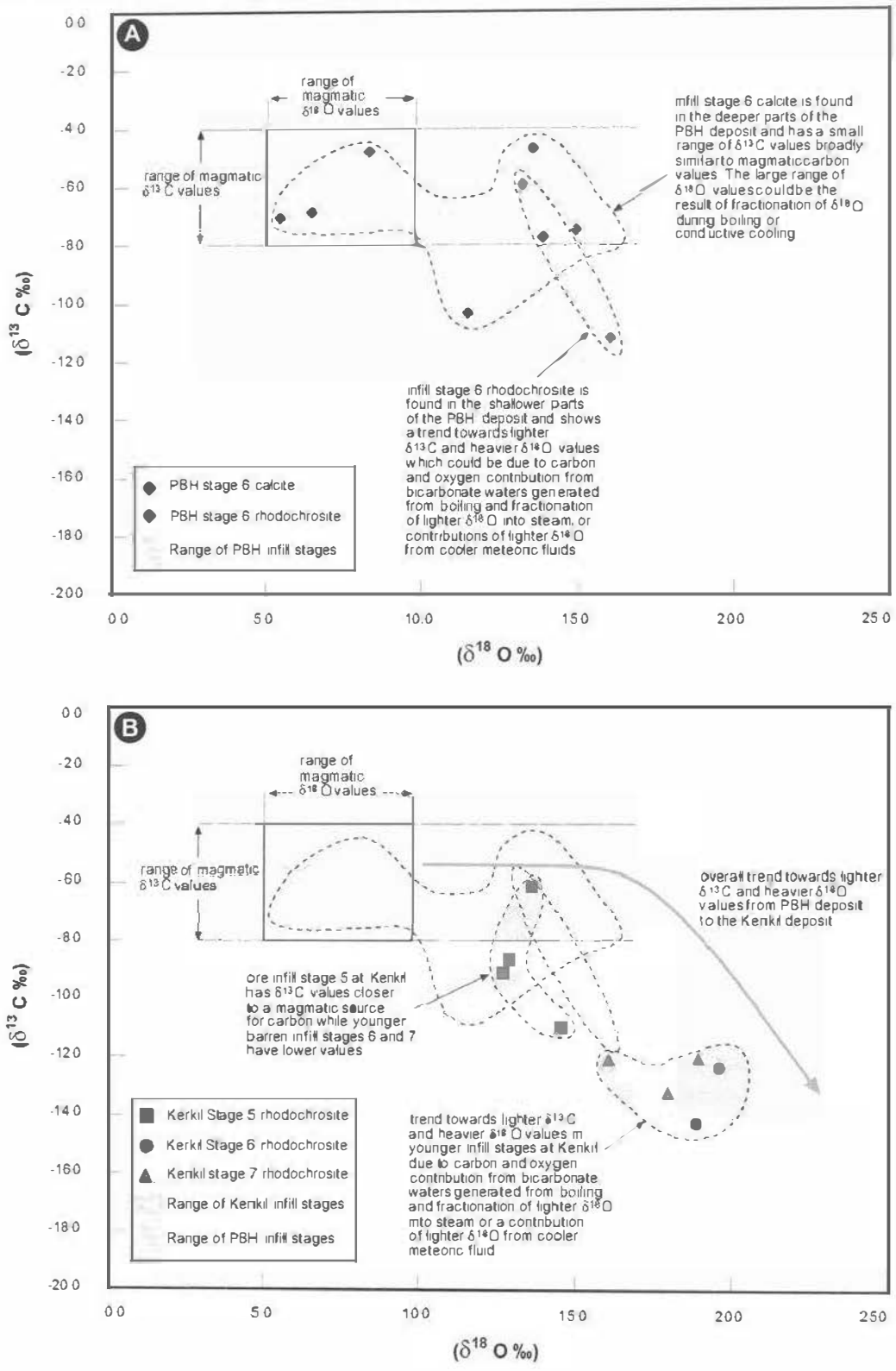

Figure 8.3 Plot of PBH and Kerikil $\delta^{13}C$ and $\delta^{18}O$ data for carbonate infill stages

A PBH: Carbonate samples from PBH consist mostly of calcite with only two samples of rhodochrosite. The $\delta^{13}C$ values of carbonate infill stages have a range broadly consistent with a magmatic source for carbon. $\delta^{18}O$ values range from values consistent with magmatic oxygen to much lower values, possibly attributed to temperature variation or fractionation of $\delta^{18}O$ during boiling.

B Kerikil: Carbonate samples from Kerikil consists entirely of rhodochrosite. $\delta^{13}C$ data for stage 5 carbonate are consistent with values of associated volcanic rocks. There is a trend towards higher carbon and lower $\delta^{18}O$ values in the later infill stages, consistent with temperature changes or fractionation during boiling.

with a relatively narrow range of $\delta^{13}C$ values (consistent with magmatic carbon source) cannot be attributed to any spatial zonation. Instead, this variation may be due to differences in depositional temperatures and/or the nature of the source fluid at the time of mineral precipitation (Fig. 8.3). In contrast to Kerikil (see below), the PBH carbonate data are quite variable. Some samples occur on a general trend with lower $\delta^{13}C$ values and higher $\delta^{18}O$ values that is consistent with equilibrium fractionation between HCO_3^- and calcite (Fig. 8.4 A). However, the scatter in the other data points suggests either wallrock exchange and/or equilibrium with H_2CO_3. There are several mechanisms for carbonate precipitation in epithermal systems, including formation from bicarbonate waters produced in the cap zone above an epithermal system (which have migrated down through faults subsequent to the collapse of the hydrothermal system; Simmons et al., 2000), and/or or by the precipitation of carbonate during boiling and the exsolvation of CO_2 (generated by magmatic degassing from deep in the hydrothermal system; Simmons and Christenson, 1994). The scatter in the PBH carbonate data cannot exclude either possibility, although the lack of significant ^{13}C depletion argues against formation from bicarbonate fluids in the steam-heated zone.

At Kerikil, the trend towards lower $\delta^{13}C$ values and higher $\delta^{18}O$ values is better defined and highlights a distinct transition in stages 5 to 7 (Fig. 8.3 and 8.4). This transition is of particular significance since Stage 5, which has $\delta^{13}C$ values consistent with magmatic carbon source (of 4 to 8‰) is one of the Kerikil ore stages, but stages 6 and 7 are not ore-bearing. The trend apparent in the stable isotope data for the carbonate samples can be attributed, at least in part, to equilibrium fractionation of calcite and HCO_3^- aqueous species from a relatively $\delta^{13}C$ depleted bulk fluid composition (Fig. 8.4B). (Note that kinetic data is not currently available for rhodochrosite and thus the reactions used to generate the fractionation curve in Figure 8.4 are based on data for calcite). The HCO_3^- is the dominant aqueous carbonate species under near-neutral to basic pH conditions (Fig. 8.5) and forms from aqueous carbonate (as bicarbonate) according to the reaction:

$$H_2CO_3 = HCO_3^- + H^+$$

During boiling, carbonate minerals can precipitate according to the reaction:

$$2HCO_3^- + Ca^{2+} = CaCO_3 + CO_2 + H_2O$$

This reaction likely closely approximates the deposition of carbonate (as rhodochrosite)

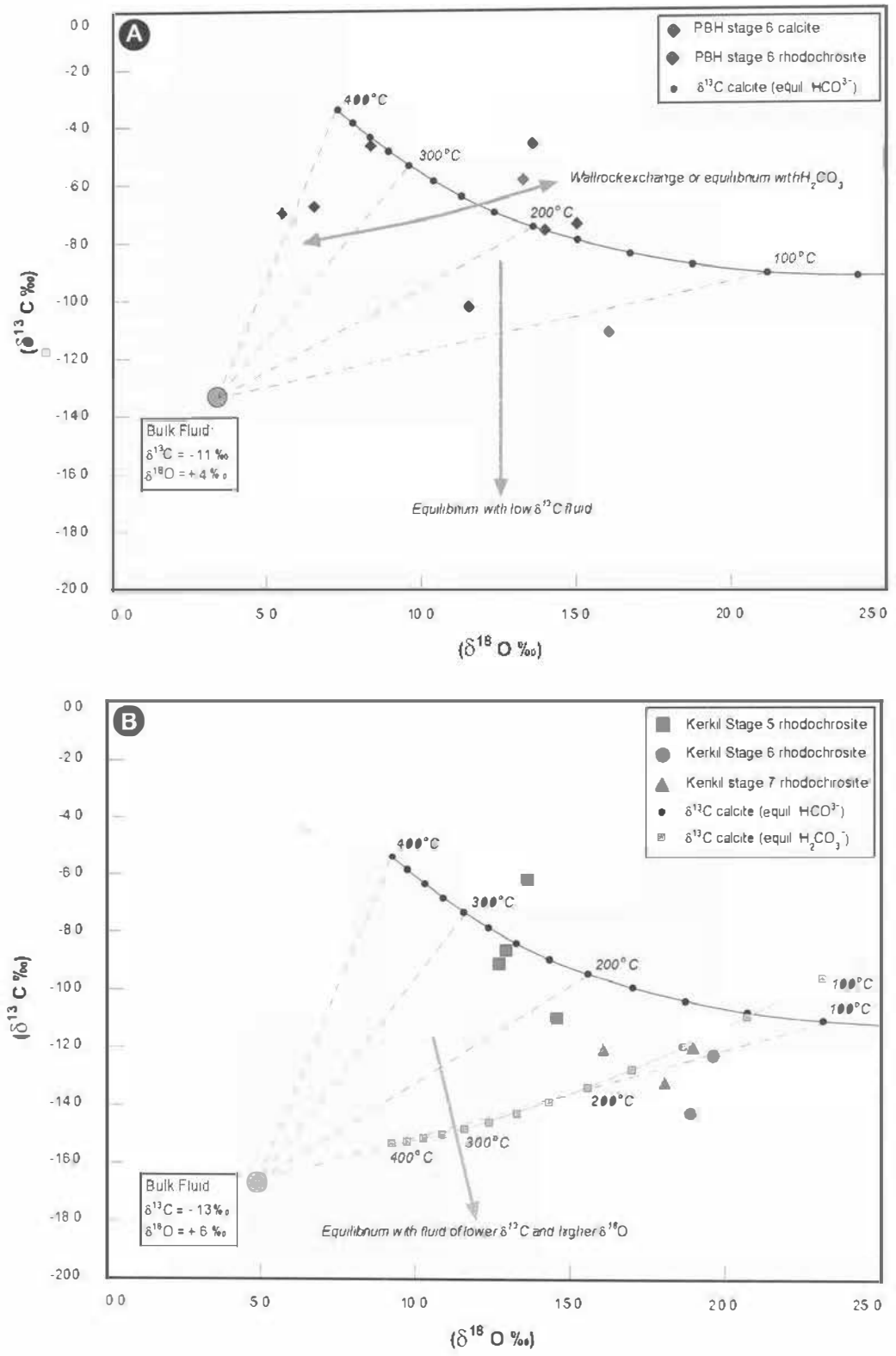

Figure 8.4 Equilibrium calcite--HCO_3^- $\delta^{13}C$ and $\delta^{18}O$ fractionation compared to Mt Muro carbonates

A PBH: Carbonate samples exhibit a range of isotope values. Some samples exhibit a trend of increasing $\delta^{18}O$ with decreasing $\delta^{13}C$ values that may be attributed to equilibrium HCO_3^- fractionation. Fractionation curves calculated using equilibrium equations of Field and Fifarek (1985) at the specified bulk fluid composition.

B Kerkil: Carbonate samples generally trend towards higher $\delta^{18}O$ and lower $\delta^{13}C$ values in the later infill stages. Fractionation curves are calculated as above, at the specified bulk fluid composition.

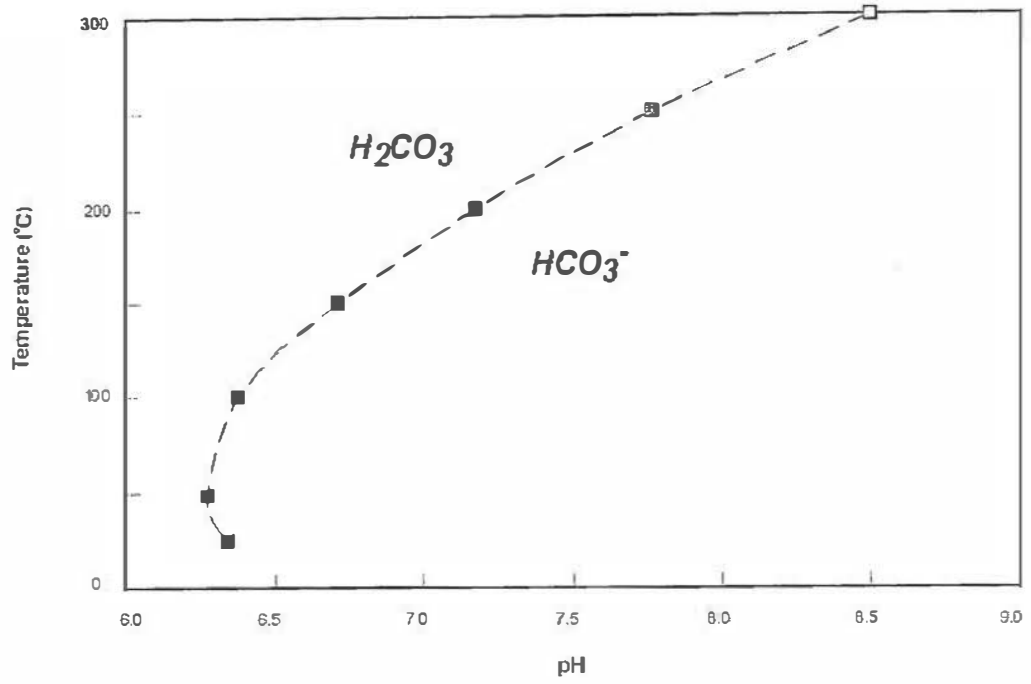

Figure 8.5 Carbonate speciation with temperature and pH

Equilibrium H_2CO_3-HCO_3^- speciation over at conditions consistent with epithermal and geothermal environments. Calculated using thermodynamic properties from SUPCRT92 (Johnson et al., 1992).

for all stages of Kerikil infill. However, data for stage 6 and 7 carbonates As shown in Figure 8.4 B, do not follow the equilibrium fractionation curve and instead are skewed towards lower $\delta^{13}C$ values. This trend cannot be attributed only to a decrease in depositional temperatures during the late infill stages, since $\delta^{18}O$ values remain relatively constant. Instead, this trend is interpreted to reflect equilibrium with late-stage CO_2-rich fluids (Fig. 8.3). This is consistent with experimental and theorectical fractionation studies that have shown progressive $\delta^{13}C$ depletion from $CaCO_3$ to HCO_3^- to CO_2. (Field and Fifarek, 1985). Empirically, a similar trend was noted in late-stage carbonates in the Geysers geothermal area (California, USA; Field and Fifarek, 1985) where measured values of the CO_2 gases (Fig. 8.2) are consistent with the $\delta^{13}C$ decrease recognized in late-stage carbonates at Kerikil. The fluids responsible for this late-stage depletion were likely bicarbonate waters produced in the steam-heated zone which have migrated down through faults subsequent to system collapse (e.g., Simmons et al., 2000).

8.3.6 Oxygen isotope results (quartz and whole rock samples)

Oxygen isotope data collected for 23 samples of quartz from vein and breccia stage infill from both PBH and Kerkil are summarized in Table 8.4. Data for 29 samples of

Table 8.4 Summary of quartz $\delta^{18}O$ data at PBH and Kerikil

Maximum, minimum and mean δ^{18}● values for quartz from PBH and Kerikil infill vein and breccia stages.

Deposit	Sample selection	n	$\delta^{18}O$ ‰ (SMOW) Min	$\delta^{18}O$ ‰ (SMOW) Max	$\delta^{18}O$ ‰ (SMOW) Mean	$\delta^{18}O$ ‰ (SMOW) Standard Deviation	$\delta^{18}O$ ‰ H_2O (SMOW) Calculated $\delta^{18}O_{H2O}$*
All		**23**	**7.1**	**12.4**	**9.5**	**± 1.2**	
PBH	**all PBH infill stages**	**10**	**7.9**	**12.4**	**9.7**	**± 1.6**	**0.7**
	infill stage 1	2	11.9	12.4	12.1	± 0.3	3.1
	infill stage 2	2	8.5	9.1	8.8	± 0.5	-0.2
	infill stage 3	3	9.7	11.3	10.3	± 0.9	1.3
	infill stage 4	1	8.5	8.5	8.5	0	-0.5
	infill stage 5	2	7.9	8.1	8.0	± 0.1	-1.0
Kerikil	**all Kerikil infill stages**	**13**	**7.1**	**10.0**	**9.2**	**±0.7**	**-1.0**
	infill stage 1	1	9.1	9.1	9.1	0	-1.1
	infill stage 2	4	8.9	9.9	9.3	± 0.4	-0.9
	infill stage 3	1	10.0	10.0	10.0	0	-0.2
	infill stage 5	1	9.7	9.7	9.7	0	-0.5
	infill stage 6	1	9.9	9.9	9.9	0	-0.3
	infill stage 7	1	9.4	9.4	9.4	0	-0.8
	infill stage 8	2	9.4	9.5	9.5	0	-0.7
	infill stage 9	2	7.1	8.8	7.9	± 1.1	-2.3

* Calculated $\delta^{18}O_{H2O}$ in equilibrium with quartz based on fractionation equation of Clayton (1992) at temperatures estimated from average fluid inclusion measurements (i.e., 250°C for PBH and 225°C for Kerikil).

whole rock powders from different alteration facies at the two deposits are summarized in Table 8.5. Full analytical details are provided in Appendix 9.

8.3.7 Oxygen isotope composition on PBH infill stages

Quartz sampled from stages 1 through 5 at PBH have $\delta^{18}O$ values ranging from 7.9 to 12.4‰ with a mean of 9.7 ‰ (Table 8.4 and Fig 8.6). There is a trend towards progressively lighter $\delta^{18}O$ values from the earliest to the latest infill stages, with mean $\delta^{18}O$ values of 12.1 ‰ in stage 1 and 8.0‰ in stage 5 (Fig. 8.6). This trend is reversed in the carbonate infill of stage 6, with $\delta^{18}O$ ranging from 5.5 to 15.0‰ with a mean of 10.6‰.

The occurrence of lighter $\delta^{18}O$ values for quartz in the later paragenetic stages cannot be attributed to depth variations, since all samples were selected from the same level in the deposit. Other possible explanations for the trend include an increase in temperature, equilibration with the andesite host rocks (with $\delta^{18}O$ values between 7.0 to 9.0 ‰), or the involvement of a lighter $\delta^{18}O$ source, such as meteoric water (present day estimated meteoric water composition at Mt Muro is equivalent to $\delta^{18}O$ = -6 ‰; Bowen and Wilkinson, 2002). A temperature increase can be precluded as a likely cause of the trend, since the mineralogy and character of associated alteration assemblages suggest that there is a decrease in temperature from stages 1 through 5 (details see Chapter 7). A larger component of meteoric water in the system as magmatic input wanes is the favored alternative for the decrease in $\delta^{18}O$ values.

8.3.8 Oxygen isotope composition of quartz from Kerikil infill stages

$\delta^{18}O$ data for samples of Kerikil quartz, sampled from infill stages 1 through 9 (but excluding stage 4), are summarized in Table 8.4 and Fig 8.6. These values range from 7.1 to 10.0‰ (with a mean of 9.2 ‰) and are relatively constant from stages 1 to 8. $\delta^{18}O$ values only become significantly lighter in the last vein stage, with values down to 7.1‰. The $\delta^{18}O$ values determined for carbonate from infill stages 5 to 7 are also shown on Figure 8.6 for comparison.

Consistent $\delta^{18}O$ values in quartz from stages 1 through 8 are thought to reflect equilibration with the andesite host rocks (characterized by whole rock $\delta^{18}O$ values between 7.0 to 9.0 ‰). The occurrence of lower $\delta^{18}O$ values for quartz in the latest

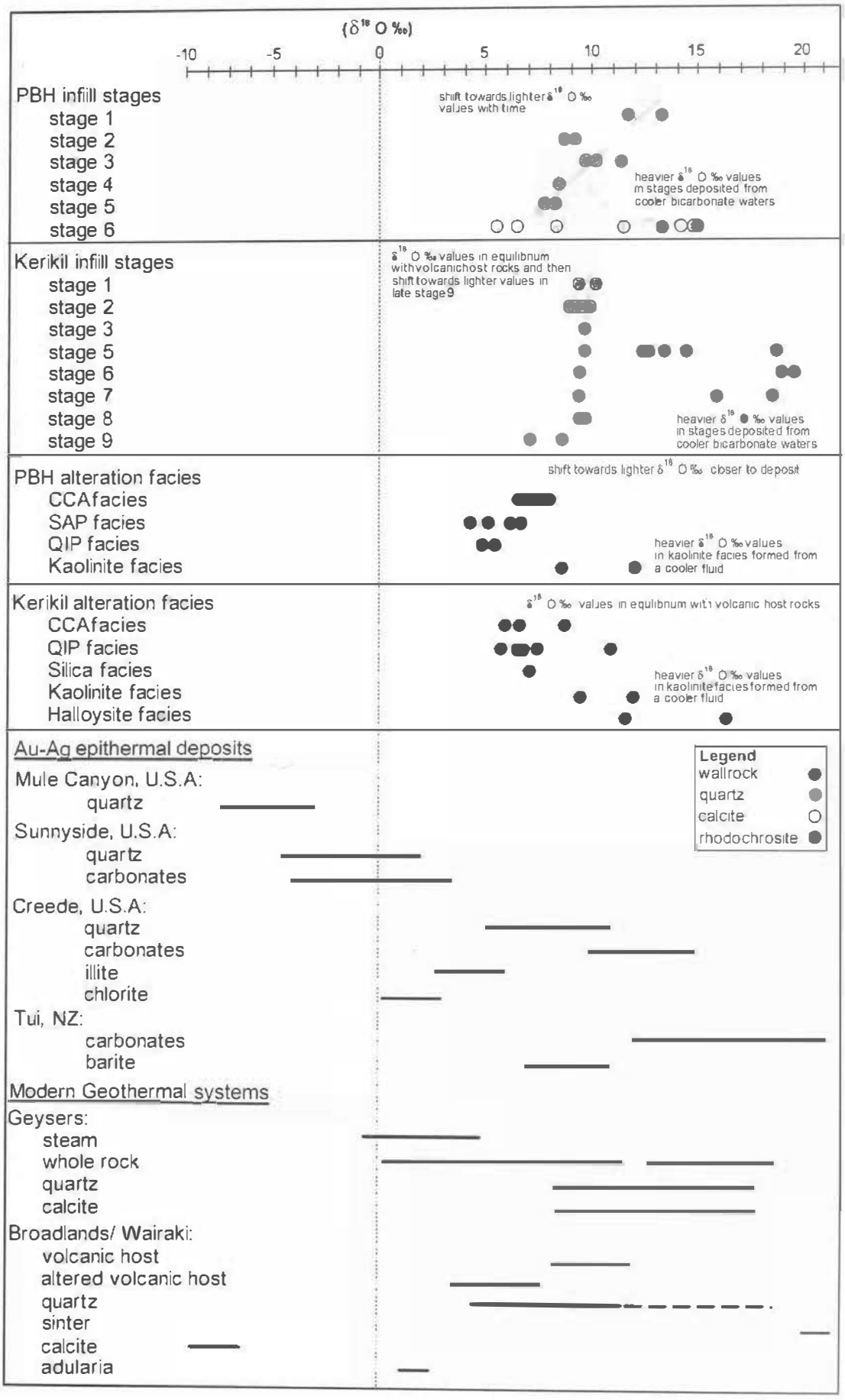

Figure 8.6 $\delta^{18}O$ data for quartz and altered host rocks from PBH and Kerikil compared with selected ancient epithermal and modern geothermal systems

$\delta^{18}O$ data for samples of quartz and whole rock powders (from alteration facies) for both PBH and Kerikil. Also shown is the range of $\delta^{18}O$ data for Au-Agdeposits and modern geothermal systems (from Field and Fifarak, 1985, John et al., 2003).

paragenetic stage cannot be attributed to depth variations, since all samples were selected from the same level in the Kerikil deposit. Alternatively, the lighter values determined for stage 9 may reflect the involvement of a hotter fluid or lighter $\delta^{18}O$ source, such as meteoric water. However, the presence of marcasite and low temperature alteration assemblages associated with the final vein stage suggest that there is a decrease, rather than an increase, in temperature associated with the final vein stage. Based on the carbonate isotope results discussed above, it is likely that the variation in quartz $\delta^{18}O$ in the final infill stages reflects the incursion of meteoric waters (specifically bicarbonate waters produced in the steam-heated zone) in the final stages of the hydrothermal system.

8.3.9 PBH alteration facies whole rock oxygen isotopes

As described in Chapter 7, alteration at PBH is zoned from distal CCA and SPA facies (at tens to hundreds of meters away from mineralization) to proximal QIP alteration only meters from the veins. A late phase of kaolinite alteration locally overprints the proximal alteration. Both the alteration zonation and overprinting relationships are reflected in whole rock $\delta^{18}O$ values for alteration assemblages, as summarized in Table 8.5.

In general, results from the PBH alteration facies indicate that there is a trend

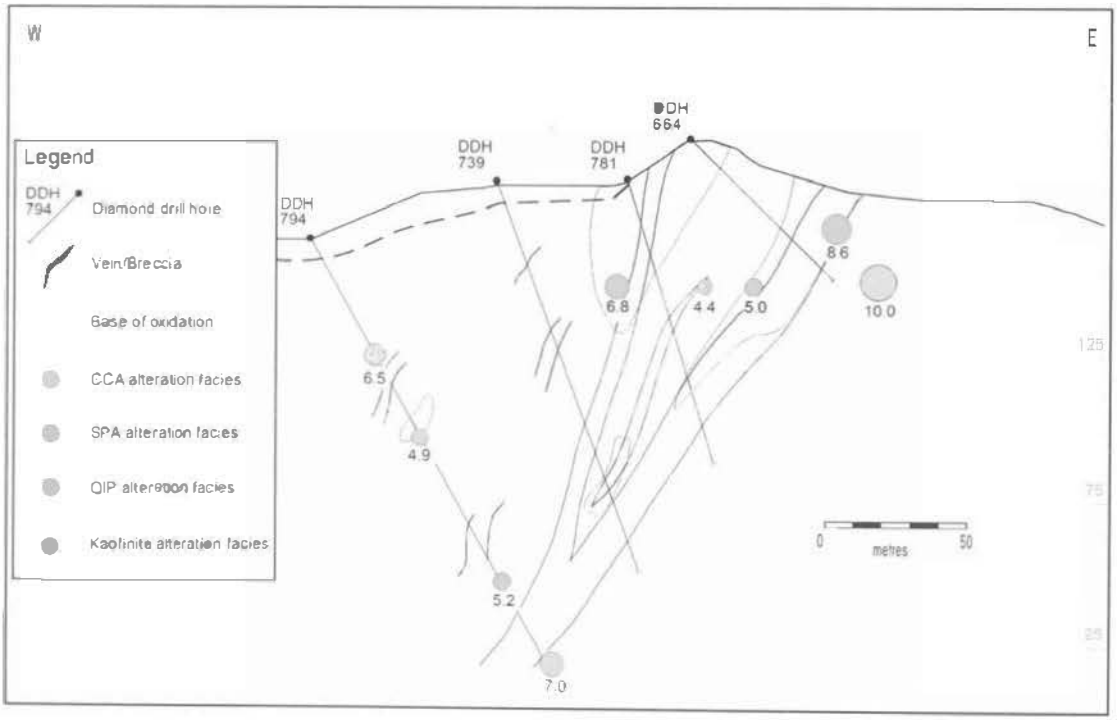

Figure 8.7 PBH cross section 12 000N showing whole rock $\delta^{18}O$ data for different alteration facies

Whole rock $\delta^{18}O$ data for alteration facies at PBH showing shift from lower values proximal to the vein and higher values associated with late stage kaolinite overprint. Shaded region marks the area of > 5 g/t Au (refer to Fig. 3.15 B, 6.3 and 7.16 B for details of geology, alteration and metal zoning)

towards lighter $\delta^{18}O$ values with proximity to mineralization. This trend is illustrated in Figure 8.7, which shows $\delta^{18}O$ values for alteration facies along section 12 000 N. The QIP facies proximal to the vein exhibits lighter $\delta^{18}O$ values (5.1 to 5.5‰) than least altered CCA facies in the footwall ($\delta^{18}O$ values of 7 to 10‰). Late kaolinite alteration in footwall fault gouge has heavier $\delta^{18}O$ values (about 9‰).

Isotope values for the least altered rocks are consistent with average values for andesitic host rocks (7.0 to 9.0 ‰). The $\delta^{18}O$ shift proximal to the vein is attributed to interaction of the host rock with either a hotter fluid or depleted $\delta^{18}O$ source (such as meteoric water). The late overprint of higher $\delta^{18}O$ values in the kaolinite facies is likely the result of cooler acid sulfate waters migrating into the system, as indicated by the alteration studies described previously (Chapter 7).

8.3.10 Kerikil alteration facies whole rock oxygen isotopes

Alteration at Kerikil is zoned on a broad scale from distal CCA facies (at tens to hundreds of meters from mineralization) to proximal QIP facies alteration next to the veins and breccia zones. However, a late phase of proximal kaolinite and halloysite alteration largely obscures and overprints earlier alteration assemblages. These relationships, and the absence of well-developed alteration zonation, is reflected in whole rock $\delta^{18}O$ values for different alteration types (Table 8.5)

In general, there are no significant trends in $\delta^{18}O$ values from the distal CCA and silica alteration zones to the proximal QIP facies, although the late-stage overprinting kaolinite and halloysite assemblages do display significantly higher $\delta^{18}O$ values (approximately 11 to 12‰; Fig. 8.8). A spatial distribution in $\delta^{18}O$ values is evident along section 20 000 E at Kerikil (Fig. 8.8), although the trend reflects progressively lighter values with increasing depth in the deposit and appears to be independent of alteration type.

The consistent $\delta^{18}O$ values of approximately 9.0‰ for the CCA, QIP and silica alteration assemblages at Kerikil are interpreted to reflect isotopic equilibration with andesitic host rocks. The shift towards higher $\delta^{18}O$ values in the overprinting kaolinite and halloysite facies may be due to the migration of cooler waters back into the hydrothermal system after the main mineralizing and alteration events, as suggested by the alteration and mineralization studies described previously (Chapters 5 and 7).

Table 8.5 Summary of whole rock $\delta^{18}O$ data for PBH and Kerikil alteration facies

Maximum, minimum and mean $\delta^{18}O$ values for whole rock powders from PBH and Kenkil alteration facies.

Deposit	Sample Selection	n	$\delta^{18}O$ ‰ (SMOW) Minimum	$\delta^{18}O$ ‰ (SMOW) Maximum	$\delta^{18}O$ ‰ (SMOW) Mean	$\delta^{18}O$ ‰ (SMOW) Standard Deviation
All		**29**	4.4	16.2	**7.9**	± 2.7
	all CCA facies	10	4.9	10.1	7.3	± 1.7
	all SPA facies	4	4.4	11.0	6.8	± 2.3
	all QIP facies	7	5.1	7.7	6.2	± 1.0
	all silica facies	1	6.1	6.1	6.1	0
	all kaolinite facies	4	8.6	12.3	10.6	± 1.8
	all halloysite facies	3	9.6	16.2	12.2	± 3.5
PBH	**all alteration facies**	**15**	4.4	**12.3**	**7.2**	± 2.1
	CCA facies	7	4.9	10.1	7.6	± 1.6
	SPA facies	4	4.4	6.8	5.7	± 1.2
	QIP facies	2	5.1	5.5	5.3	± 0.4
	kaolinite facies	2	8.6	12.3	10.5	± 2.6
Ketikil	**all alteration facies**	14	**5.1**	**16.2**	**8.7**	**± 3.1**
	CCA facies	3	5.1	8.9	6.6	± 2.0
	QIP facies	5	5.9	11.0	7.6	± 2.0
	silica facies	1	6.1	6.1	6.1	0
	kaolinite facies	2	9.4	12.0	10.7	± 1.8
	halloysite facies	2	10.7	16.2	13.5	± 3.9

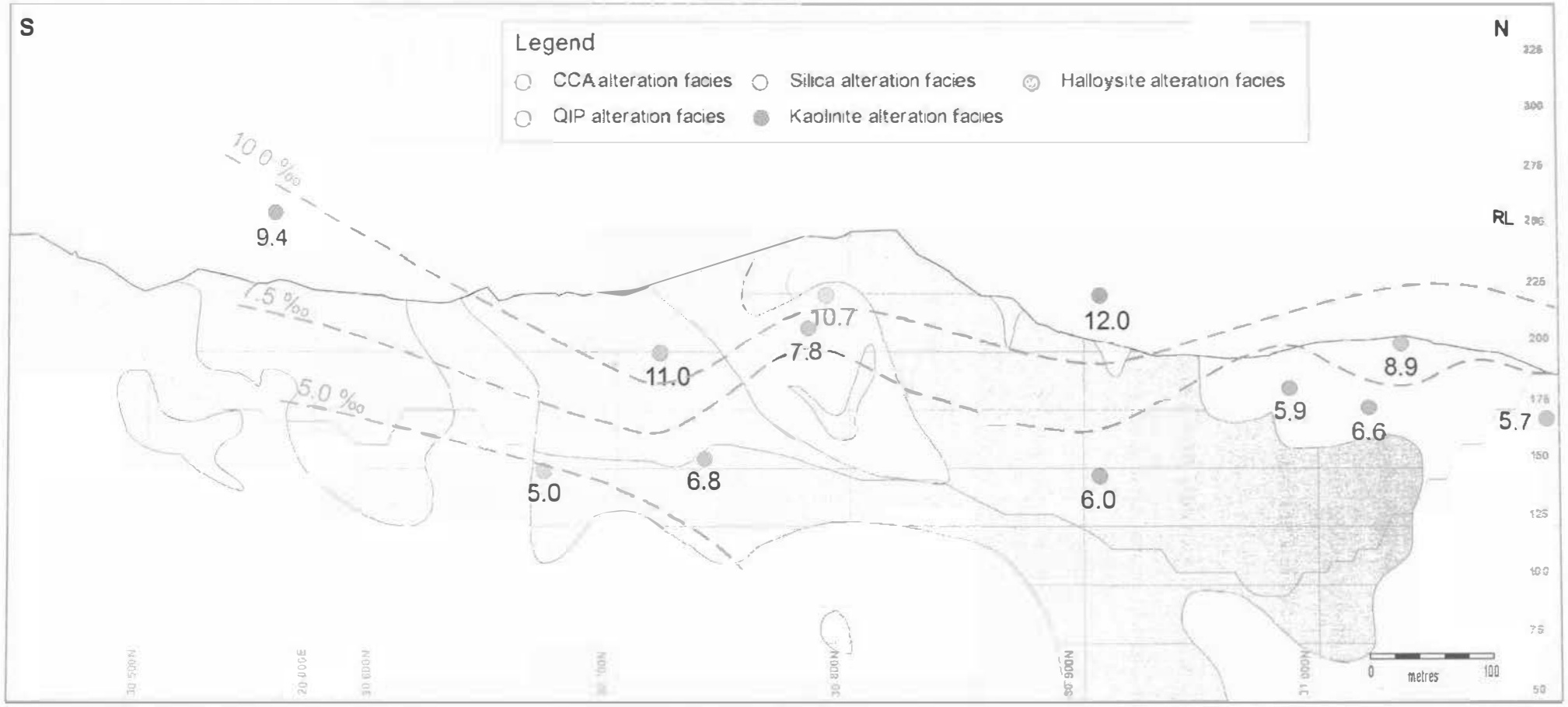

Figure 8.8 Kerikil 20 000E long section with hand-contoured whole rock $\delta^{18}O$ values for different alteration facies

Whole rock $\delta^{18}O$ data for alteration facies at Kerikil 2 showing a shift towards lower values with depth along the north-northwest Kerikil 2 structure, independent of alteration facies mineralogy. Some results are projected from off section (within 50 m). Shaded region marks the area of > 5 g/t Au

8.4 Summary

Fluid inclusions data for the Mt Muro deposits indicate that mineralizing fluids at PBH were hotter than those at Kerikil, and that the PBH veins formed at deeper levels (Simmons and Browne, 199●). There is evidence for boiling at both deposits and some inclusions at Kerikil suggest sealing, over-pressurization and hydraulic rupture (Simmons and Browne, 199●).

Sulfur isotope data from sulfides in the Mt Muro deposits occur over a narrow range of –1 to +4‰. These values are similar to those in modern geothermal systems and are consistent with a magmatic sulfur source.

Carbonate $\delta^{13}C$ and $\delta^{18}O$ data for the two deposits suggests varying depositional conditions. At Kerikil, there is a trend towards heavier values $\delta^{13}C$ values with progressively later infill stages. This trend can be attributed, at least in part, to precipitation from a HCO_3^- dominant fluid at near-neutral to basic pH conditions, likely caused by boiling of hydrothermal fluids. Further ^{13}C depletion is consistent with the incursion of a CO_2-rich fluid in the late-stages of the hydrothermal system; most likely bicarbonate waters generated in a steam-heated zone, which is inferred to have overlain the deposit. Isotope data for PBH carbonates are more scattered than the Kerikil dataset, suggesting a variety of depositional processes including precipitation from CO_2 generated by magmatic degassing from deep in the hydrothermal system and precipitation from HCO_3^- dominant fluids (derived from boiling). Rhodochrosite from both deposits is enriched in $\delta^{18}O$ relative to calcite, suggesting that it may form from a highly fractionated fluid developed as a result of boiling. This is consistent with the spatial distribution of rhodochrosite at PBH and Kerikil which is found in the shallower parts of the deposits and therefore most likely to have interacted with high level bicarbonate waters.

Oxygen isotope data for quartz across all infill stages at PBH and Kerikil are similar to average $\delta^{18}O$ values for volcanic host rocks (approximately 7 to 9‰). This suggests that fluids in both deposits had reached isotopic equilibrium with the host rocks. At PBH, oxygen isotope data show a trend towards lighter values with progressively younger infill stages. This trend likely reflects a progressive increase in meteoric water contribution to the hydrothermal system and/or fractionation due to varying source fluids. At Kerikill,

however, a similar trend is not apparent and $\delta^{18}O$ values are relatively consistent across infill stages 1 though 8 with values similar to the mean composition of volcanic host rocks. This relationship suggests that the fluids responsible for alteration and mineralization maintained isotopic equilibrium with the host rocks. These conditions likely reflect a system in which extensive water-rock interaction occurs via sealing of the system and subsequent brecciation allows maximum contact with host rocks. Significantly lighter $\delta^{18}O$ values in the final paragenetic infill stage is attributed to the influx of cool meteoric waters.

Oxygen isotope data from whole rock analyses of different alteration facies at both PBH and Kerikil reflect the zonation patterns described previously in Chapter 7. At PBH, there is a trend towards lower $\delta^{18}O$ values with proximity to the mineralized structures that likely reflects interaction with a hotter upwelling fluid. A similar zonation is not apparent at Kerikil, although both deposits have a late-stage overprint with high $\delta^{18}O$ values that is associated with kaolinite and/or halloysite alteration. This overprint is interpreted to reflect input of a cooler fluid and/or a high-$\delta^{18}O$ source fluid, possibly related to residual fluids at the top of the hydrothermal system.

Chapter 9

The Genesis of the PBH and Kerikil-Deposits

CHAPTER 9

THE GENESIS OF THE PBH AND KERIKIL DEPOSITS

9.1 Introduction

Conclusions and findings of the previous eight chapters are combined in this chapter to understand the geological history of the Mt Muro Au-Aglow sulfidation epithermal deposits and construct an ore deposit model. This model is based on studies of regional Kalimantan tectonics, volcanic architecture and geochemistry, structural setting and style, mineralization paragenesis, textures and geochemical characteristics, metal distribution and zoning, alteration paragenesis and geochemistry, and ore fluid chemistry.

The genesis of the PBH and Kerikil deposits is described in four phases; Phase 1: Volcanic emplacement and structural setting; Phase 2: Hydrothermal system evolution and ore deposition; Phase 3: Late stage magmatism; and Phase 4: Uplift, weathering and erosion.

9.2 Phase 1: Volcanic emplacement and structural setting

The Central Kalimantan Arc is a northeast trending volcanic arc of andesitic and basaltic composition that developed above a southward dipping Benioff zone in the Early to Late Cenozoic (Fig. 9.1 A). The predominately andesitic and basaltic volcanic rocks (correlated with the Sintang and Metalung suites) hosting Mt Muro were emplaced as part of the arc in the Late Oligocene to Early Miocene (Fig. 9.2 A).

At least one (and perhaps several) andesite stratovolcanos formed along a northeast trend in the Mt Muro region in the Late Oligocene to Early Miocene. Interlayered coherent andesite lavas, non-stratified monomict andesite breccia (autobreccias) and tuffs recognized at PBH formed in the volcanic slope environment, and the thick coherent andesite lavas and poorly sorted clast supported polymict breccia facies (talus breccias) at

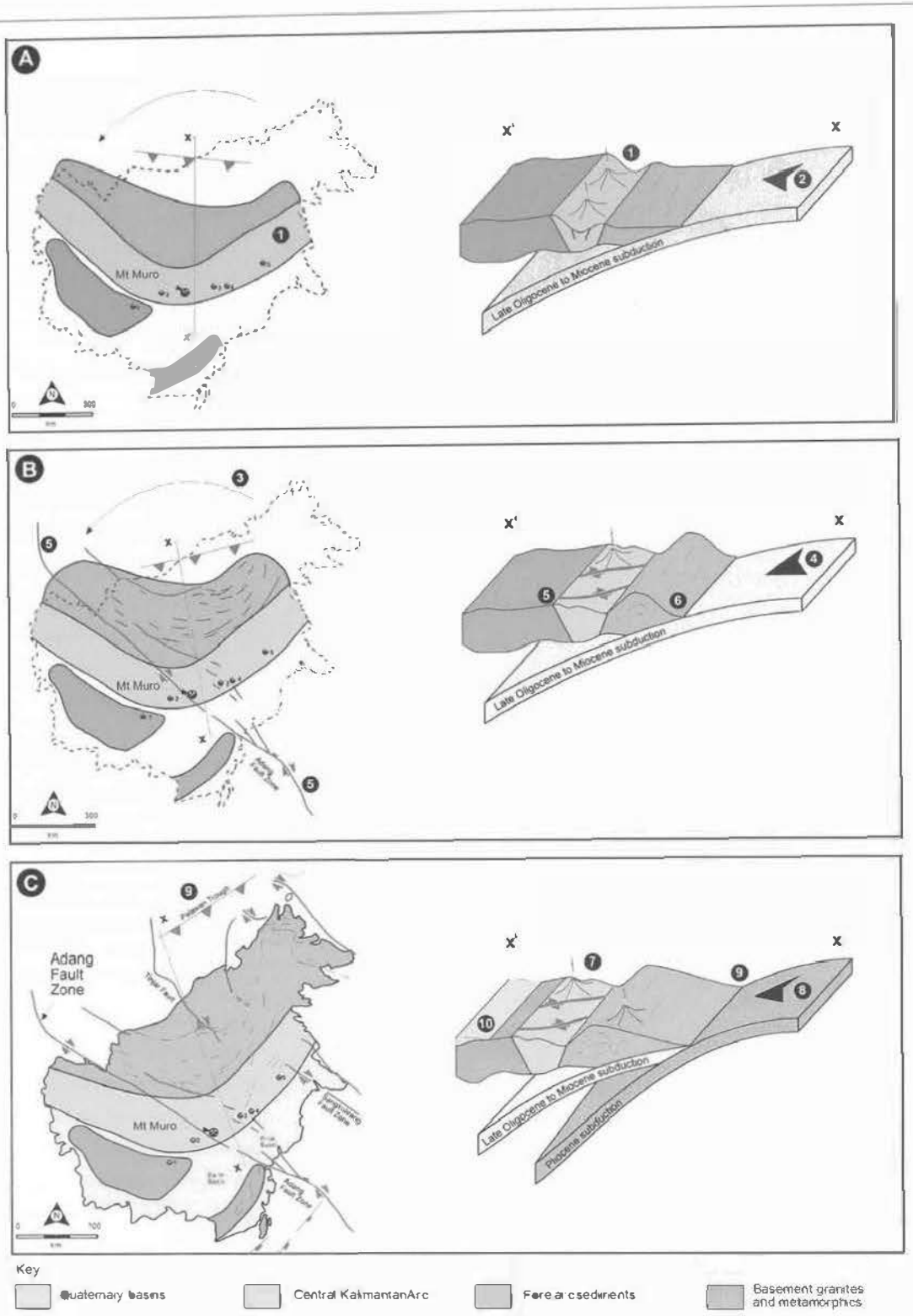

Figure 9.1 Schematic tectonic evolution and rotation of Borneo

Simplified geology and tectonic features of Borneo showing major tectonic domains. Also shown are the locations of Mt Muro and other major epithermal ore deposits aligned along the Central Kalimantan Arc and Kalimantan Gold Belt. Key to deposits marked by mine symbols: 1 = Mirah, 2 = Marsupa Ria, 3 = Kelian, 4 = Muyup and 5 = Busang.

A Andesitic to basaltic magmatism associated with the Central Kalimantan Arc (1) formed by back-arc spreading above a southward dipping Benioff zone (2) in the Late Oligocene to Mid Miocene.

B Rotation of stress field and change in subduction trajectory occurred in the Middle Miocene (3) and (4). This is followed by basin inversion and activation of major northwest faults, such as the Adang Fault Zone (5). Closure of the fore arc basin resulted in folded and uplifted sediments in the fore-arc wedge (6).

C Pliocene basaltic magmatism (7) is associated with subduction in the Palawan Trough (8 and 9). Quaternary sedimentation occurred in the Kutai and Barito Basins (10).

Figure 9.2 Phase 1, 2 and 3 Volcanic and structural setting of M1 Muro mineralization.

A Andesitic volcanism occurs along the northeast trending Central Kalimantan Arc in the Late Oligocene and continues in the Mid Miocene. Andesitic volcanism at Mt. Muro is emulated with Stirling volcanism. (1) Andesitic stratovolcanoes are formed at Mt Muro. (2) and (3) Deposition of proximal steep facies including coherent andesite lavas, non-stratified monomict andesite breccia and tuffs at PBH. (4) Central vent facies consisting of steeply dipping coherent andesite lavas and coherent basaltic andesite intrusions (dyke and sheeted).

B Extension associated with back arc spreading in the Miocene. (5) Northwest trending grabens formed in response to northeast directed extension. Medial valley fill deposition occurs at Bukit Balimbing. (6) Poorly sorted clast supported polymict breccia facies (talus breccias) shed off northwest sinking fault scarps at Kerikil. (7) Coherent basalt lava flows, poorly sorted clast supported polymict breccia facies (debris breccia), tuffs and coherent andesite lavas deposited in northwest trending grabens.

C North-south compression, basin inversion and formation of north-south trending pull-apart basins are formed in the Mid Miocene. (8) Dextral movement on northwest sinking graben structures associated with Mid Miocene intrusion event. (9) North-south trending pull-apart basin formed as a response to dextral movement on northwest sinking structures, distal basin fill environment of deposition. (10) Uplift and unroofing of volcanic underlying sediments into the pull apart basin. (11) Sub-aerial to shallow sub-aqueous braiding (?) setting with terrestrial sediment input. (12) Coherent andesite lavas, lapilli tuffs and non-stratified sediment matrix supported breccia (andesite hyaloclastite) deposited.

D Reversal of north-south compressive stress and consequent dilation of north-south striking faults in the Mid to Late Miocene. (13) Dextral movement on northwest trending graben structures associated with Mid Miocene intrusion event. (14) Andesite volcanism has waned or ceased. (15) Folding in northwest orientated graben indicating north-south compression. (16) Dilation of north-south striking faults and formation of poorly sorted rounded polymict milled breccia facies (maar breccias) at Tulubu.

E Reversal of north-south compressive stress and consequent dilation of northwest-south striking faults in the Mid to Late Miocene. (17) Dextral movement on northwest graben sinking structures associated with Mid Miocene intrusion event. (18) Dilation of north-south striking faults and formation of synsedimentary dilation veins at PBH. (19) PBH deposit is controlled by pre-existing basin structures and in turn developed in response to Reidel type mechanics. (20) North-south striking dilation structures developed in response to Reidel type mechanics at Kerikil. (21) Kerikil deposit hosted by brittle impermeable coherent andesite lavas and coherent basaltic andesite intrusions of the central vent environment host rocks. (22) Younger basaltic andesite dikes emplaced along northwest striking structures at Permata.

F Late basaltic volcanism associated with Plio-Pleistocene Mesalong volcanism. (23) Late northeast striking basaltic dikes at Permata. (24) Formation of Kumbang basaltic cinder cone volcano. (25) Plateau basalts cover all earlier volcanism and some sections of the vein structures.

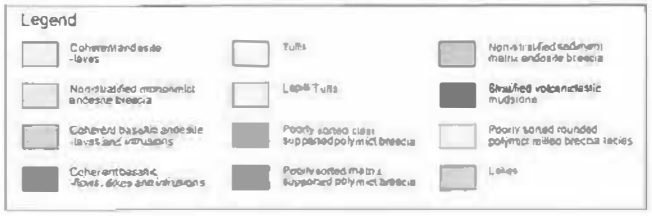

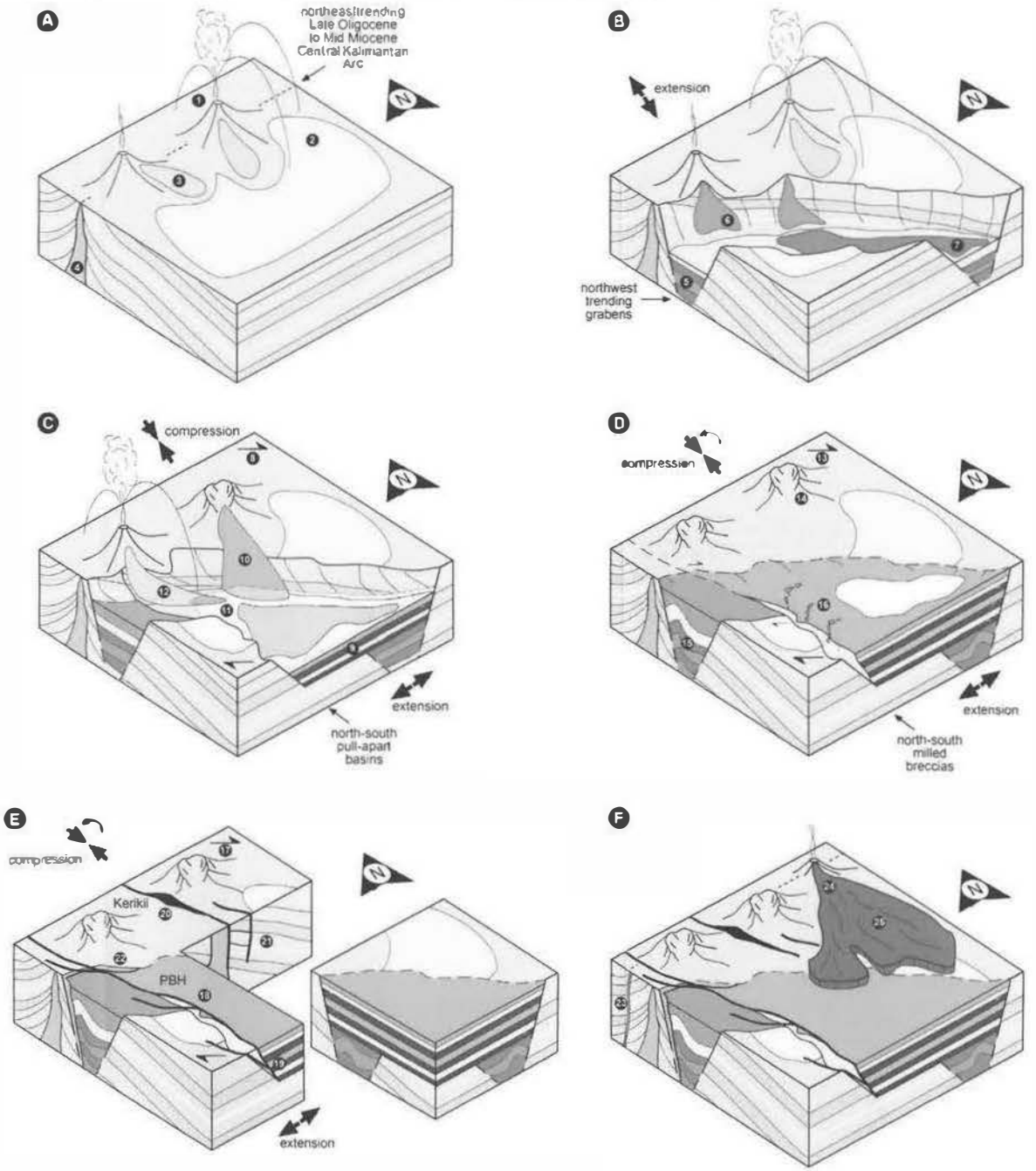

Kerikil formed in the central vent environment (Fig. 9.2 A). Northwest trending grabens formed in response to northeast extension and dilation of northwest striking faults. The valley fill facies at PBH were deposited into the northwest striking grabens and poorly sorted clast supported polymict breccia facies (talus breccias) at Kerikil was shed of northwest striking fault scarps (Fig. 9.2 B). Realignment of the stress field (Fig. 9.1 B) (associated with a 15° island scale rotation of Borneo initiated in the Early to Mid Miocene) and north-south compression is expressed as dextral movement on northwest striking faults. Regionally, the Adang Fault Zone exhibits the same dextral sense of movement in response to tectonic reorganization (Fig. 9.1 B). On a district-scale, this dextral movement opened up north-south orientated pull apart basins (Fig. 9.2 C). Mature sediments were eroded from uplifted areas and deposited into these basins (represented by the distal basin facies at PBH). At least part of the pull-apart basin units were deposited under sub-aqueous conditions as indicated by the occurrence of non-stratified sediment matrix supported breccia facies (andesite hyaloclastite) and stratified volcaniclastic mudstone (with fossil worm burrows and tree fragments).

The onset of hydrothermal activity in the Mt Muro area is recognized by the emplacement of north-south trending, hydrothermal, poorly sorted, rounded, polymict, milled breccia facies (maar breccia) dikes at PBH along dilated, pre-existing, north-south striking basin structures (Fig 9.2 D). Poorly sorted rounded exotic polymict milled breccia facies (pebble breccias) at Kerikil formed along north-south and east-west striking fissures.

Continued dextral movement on northwest striking structures resulted in the dilation of north-south structures at PBH and Kerikil. This dilation provided a focus for fluids circulating in large (> 5 km diameter) hydrothermal cells (Fig. 9.2 E), which are represented by large areas of magnetite destruction. This dilation is also associated with the emplacement of basaltic andesite intrusions at Kerikil in a north-south orientation, and emplacement of northwest trending basaltic andesite dikes at PBH (Fig. 9.2 E).

Near the end of hydrothermal activity, basalt dikes were emplaced along pre-existing north-south and northeast striking structures. Late Plio-Pleistocene basaltic volcanism was correlated with the Metalung Suite, and is responsible for the youngest cinder cones and plateau basalts (Fig. 9.1 C and 9.2 F).

9.2 Phase 2: Hydrothermal system evolution and ore deposition

As noted above, hydrothermal activity at PBH and Kerikil was initiated by dextral movement on northwest striking basement structures that caused dilation of north-south and north-northwest striking structures (Fig. 9.2 E). Magmatic fluids (as indicated by sulfur and carbon isotopes values) associated with arc magmatism ascended and combined with circulating meteoric fluids (as indicated by oxygen isotopes values and dilute liquids in fluid inclusions). The large, northwest striking basement structures provided an effective conduit for magmatic fluids to enter the meteoric-dominated hydrothermal system, whereas dilational north northwest and north-south striking structures focused local meteoric fluid flow.

At PBH, the first infill stage (stage 1 jasper) formed in response to rising hot (200°-250°C) hydrothermal fluids interacting with oxidizing ground water that were present in the permeable pull-apart basin sequences (Fig 9.2 E and 9.3 A). In contrast, jasper did not form at Kerikil due to less permeable host sequences (e.g., the central vent region facies) that prevented significant interaction with oxidized meteoric fluids.

Continued dilation of the PBH and Kerikil structures provided a focus for fluid flow. High flow rates and rapid cooling of silica gels in the narrow initial fissures induced precipitation of microcrystalline quartz early in the paragenesis at PBH and Kerikil. Rapid crystallization was conducive to sealing of the fissures, which were subsequently reopened after dilation and brecciation of the seal. Illite alteration associated with these early infill stages indicate high fluid to rock ratios and interaction with a 200-250° C, near neutral fluid (Simmons and Browne, 2000). The presence of fine-grained adularia indicates boiling also occurred (Fig. 9.3 B).

Fluid flow was focused at the intersection of northwest striking and north-northwest striking structures and dilation sites along the north-northwest striking structures. At dilational sites within the conduit, the combined effects of boiling and gas loss (specifically H_2S, CO_2 and steam) resulted in physiochemical changes in the ore fluid (pH, temperature, sulfur activity and salinity), leading to metal precipitation. The deposition of gold and silver, which can be transported as bisulfide complexes, is induced by boiling (Gammons and Williams-Jones, 1995; Spycher and Reed, 1989). In contrast, the precipitation of base metals such as copper, lead and zinc (transported as chloride complexes) can be attributed

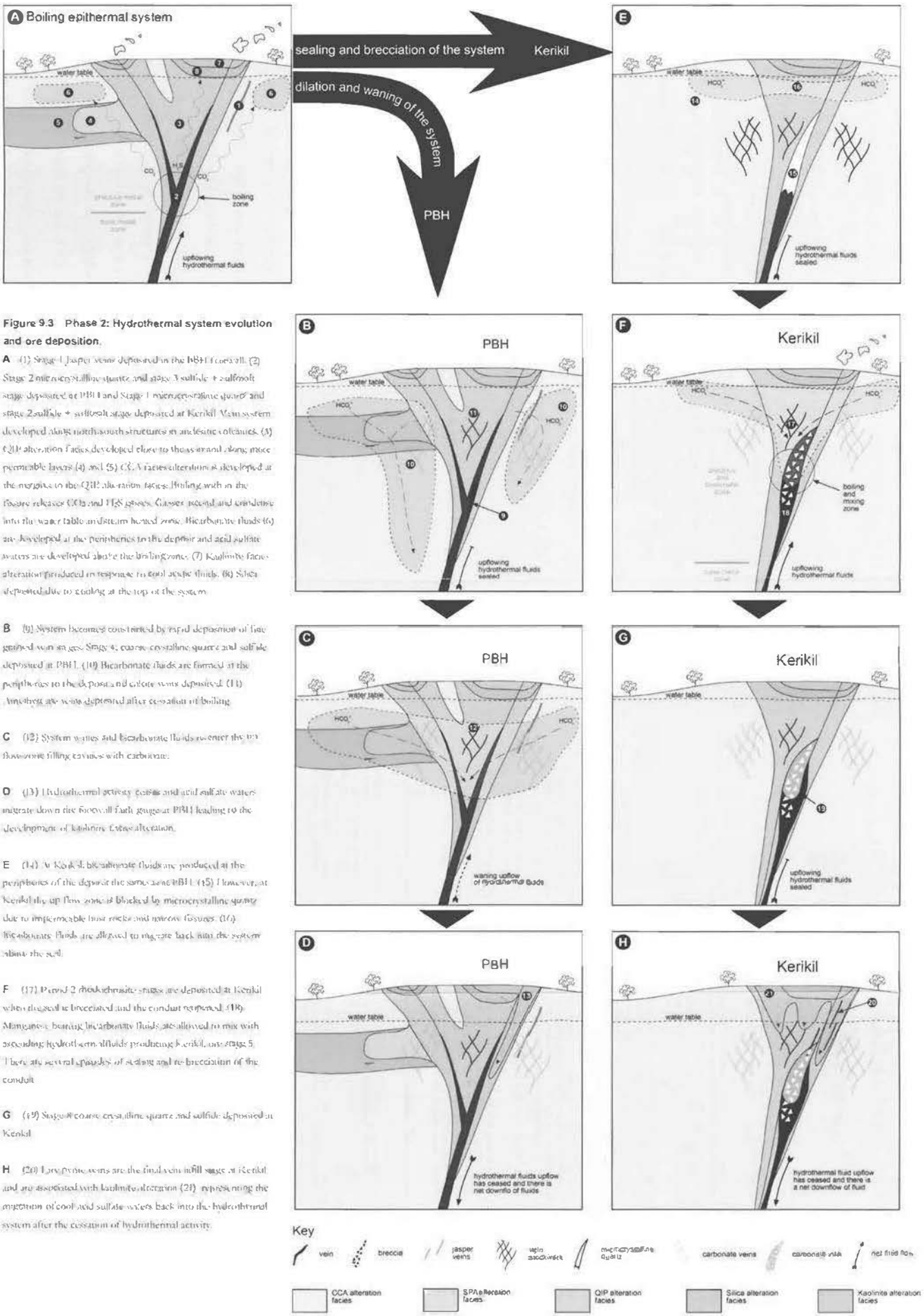

Figure 9.3 Phase 2: Hydrothermal system evolution and ore deposition.

A (1) Stage 1 jasper veins deposited in the PBH I core still. (2) Stage 2 microcrystalline quartz and stage 3 sulfide + sulfosalt stage deposited at PBH I and Stage 1 microcrystalline quartz and stage 2 sulfide + sulfosalt stage deposited at Kerikil. Vein system developed along north-south structures in andesitic volcanics. (3) QIP alteration facies developed close to the vein and along more permeable layers (4) and (5). (6) CCA facies alteration is developed at the margins to the QIP alteration facies. Boiling with in the fissure releases CO_2 and H_2S gases. Gasses ascend and condense into the water table and steam heated zone. Bicarbonate fluids (6) are developed at the peripheries to the deposit and acid sulfate waters are developed above the boiling zone. (7) Kaolinite facies alteration produced in response to cool acidic fluids. (8) Silica deposited due to cooling at the top of the system.

B (9) System becomes constricted by rapid deposition of fine grained vein stages. Stage 4, coarse crystalline quartz and sulfide deposited at PBH I. (10) Bicarbonate fluids are formed at the peripheries to the deposit and calcite veins deposited. (11) Amethyst vein deposited after cessation of boiling.

C (12) System waters and bicarbonate fluids re-enter the ore fluid zone filling cavities with carbonate.

D (13) Hydrothermal activity ceases and acid sulfate waters migrate down the footwall fault against PBH leading to the development of kaolinite facies alteration.

E (14) At Kerikil, bicarbonate fluids are produced at the peripheries of the deposit the same as at PBH I. (15) However, at Kerikil the up flow zone is blocked by microcrystalline quartz due to impermeable host rocks and narrow fissures. (16) Bicarbonate fluids are alleged to migrate back into the system above the seal.

F (17) Period 2 mesothermal stages are deposited at Kerikil when the seal is breeciated and the conduit reopened. (18) Manganese bearing bicarbonate fluids are allowed to mix with ascending hydrothermal fluids producing Kerikil ore stage 5. There are several episodes of sealing and re-brecciation of the conduit.

G (19) Stage 6 coarse crystalline quartz and sulfide deposited at Kerikil.

H (20) Late pyritic veins are the final vein infill stage at Kerikil and are associated with kaolinite alteration (21) representing the migration of cool acid sulfate waters back into the hydrothermal system after the cessation of hydrothermal activity.

to dilution and/or cooling (Barnes, 1979; Spycher and Reed, 1989). These factors are responsible for the metal zonation recognized at PBH, with precious metals occurring above the boiling zone and base metals below. The occurrence of adularia and low fineness electrum in the PBH ore stages is further evidence that boiling occurred during metal precipitation.

The formation of a steam heated cap above the Mt Muro deposits resulted from the condensation of gasses (such as H_2S and CO_2), derived from the boiling of underlying hydrothermal fluids (Fig. 9.2 A). H_2S condensates at the top of the system produced cool acid sulfate waters that were responsible for kaolinite facies alteration. Silica was deposited at the water table via cooling of the ascending silica-rich hydrothermal fluids. At the edges of the hydrothermal systems, the condensation of CO_2 into meteoric waters resulted in moderate to high temperature (200-250°C), near neutral to slightly basic, bicarbonate (HCO_3^-) waters . These waters are responsible for the development of CCA facies alteration and depletion of elements such as sodium and manganese from the volcanic host rocks.

The fine-grained ore and infill stages at PBH and Kerikil are followed by coarser mineral precipitation (Fig. 9.2 B). This transition indicate slower rates of deposition, likely related to slower flow rates or a cessation of flow rate and sealing of the hydrothermal system. Stage 4; coarse-crystalline quartz + sulfide at PBH has gold-silver telluride inclusions in pyrite that may indicate throttling and condensation of magmatic gasses. Coarse-grained amethyst in stage 5 at PBH and in stage 3 at Kerikil marks the end of the silica infill stages. This amethyst is associated with near neutral to slightly alkaline waters (Fig 9.2 B). The deposition of coarsely crystalline calcite of stage 6 at PBH and stage 4 at Kerikil marks the migration of bicarbonate waters back into the hydrothermal system and along late north east striking structures. This calcite is also recognized at the margins to the deposit, where it formed due to increasing temperature and reverse solubility as peripheral bicarbonate fluid entered into the hot up flow zone of the hydrothermal system (Fig. 9.2 C). This stage indicates encroachment of alkaline waters back into the system.

Carbonate infill marks the end of vein stage paragenesis at PBH, but the paragenetic evolution at Kerikil is more complex and additional rhodochrosite-bearing infill stages are recognized. The divergence in hydrothermal evolution between the two deposits is a result

of contrasting lithologies (and thus rheologies) of the host sequences, structural setting, and relative depth of formation. At PBH, the ore-hosting structure is favorably aligned for dilation, thus allowing the preservation of an open fluid pathway. As well, porous lithologic units (such as tuffs and lapilli tuffs) permit the lateral fluid flow when the main fluid conduit has been sealed. In contrast, impermeable host rocks at Kerikil were readily sealed due to precipitation of fine-grained infill stages. Sealing allowed bicarbonate waters back into the system above the seal, which were previously excluded due to buoyancy and out flow effects (Fig. 9.2 E). Brittle rupture of the seal occurred due to over-pressurization and/or further dextral movement on northwest striking structures (9.3 F). This rupture allowed the mixing of upwelling hydrothermal fluids with bicarbonate fluid above the seal, and subsequent mineral precipitation (e.g., stage 5; rhodochrosite + sulfosalts around jigsaw fit breccias). Selenium substitution within the sulfides, native silver precipitation, and gold-rich electrum as inclusions in pyrite, provide further evidence that oxidizing conditions and fluid mixing were important controls on mineral precipitation. High fineness electrum, as seen at Kerikil, is also produced from mixing of gold bisulfide with an oxidized fluid (e.g., Gammons and Williams-Jones, 1995; Spycher and Reed, 1989). Precious metals and base metals were deposited at the same height where conditions favorable to bisulfide and chloride complexed metal precipitation occurred (e.g., Barnes, 1979). Several episodes of sealing by microcrystalline quartz and subsequent brecciation are recognized during stage 6 at Kerikil, possibly due to rapid up flow rates and/or cooling of a silica rich fluid (on contact with cooler bicarbonate waters). The final stage is marked by coarse-crystalline amethyst and minor rhodochrosite, indicating slow cooling and rates of crystallization. Manganese required for rhodochrosite deposition in Period 2 may have been derived from altered volcanics in the steam-heated zone (e.g., Henley et al., 1986). Gradual cooling of the Kerikil hydrothermal system is marked by the deposition of coarse crystalline quartz and sulfide veins (stage 8; Fig. 9.3 G).

The final stages of both the PBH and Kerikil hydrothermal systems are marked by the migration of acid sulfate waters (formed in the steam heated cap) down along northwest striking structures at Kerikil, and in the footwall fault gauge to the north-northwest striking structure at PBH. Stage 9 pyrite veins at Kerikil are equivalent to late kaolinite and pyrite in the footwall fault gauge at PBH (9.3 D and H). At Kerikil, the

youngest northwest striking coarse grained pyrite and marcasite veins are associated with high Tl and As contents, consistent with fluids observed in the mud pool areas of modern geothermal systems (Reed and Plumlee, 1992).

9.3 Phase 3: Late stage magmatism

Late stage magmatism is limited to northeast striking basaltic dikes at PBH, the Kembang cinder cone volcano (near the Mt Muro golf course) and regional plateau basalts. This magmatism is related to recent subduction in the Palawan trough and is correlated with the youngest Pliocene Metalung Volcanics (Fig 9.1 C and 9.2 F).

9.2 Phase 4: Uplift, weathering and erosion

After cessation of magmatic and hydrothermal activity, there was a period of uplift and erosion at Mt Muro followed by a period of subsidence (associated with the Barito Basin; Fig 9.4). The height of the paleo-water table (and therefore a minimum height for the paleo-surface) was determined from fluid inclusion data, using depth pressure estimates based on samples exhibiting boiling. These measurements indicate that there was a water column of > 400m at PBH and between 225 and 400 m at Kerikil. The large range of pressure-depth boiling measurements obtained from the same RL level at Kerikil could be due to over pressurization of the system. Anomalous pressure values (equivalent to 400 m) therefore could be an over estimation. Estimates of 225 m are considered more realistic and favored in light of the position of the silica cap at 390 RL, which is also an indicator of the paleo-water table height. If paleo-water table height is known, minimum estimates for paleo-surface can be determined. Paleo-surface estimates can then be compared with present day surface level and the amount of erosion since mineral precipitation calculated. At PBH, depth pressure measurements imply a paleo-surface at a minimum of 520 RL. The silica cap at Mt Muro is at 400 RL, which compares well with the estimate for paleo-water table height. Current valleys at PBH are at 140 RL, implying there has been at least 120 to 380 m (average 200 m) of erosion at PBH.

At Kerikil, depth-pressure measurements imply a paleo-surface at a minimum of 400 RL. The silica cap at Ganung Baruh is at 390 RL, which correlates well with the estimate for paleo-water table height. Current valleys at Kerikil are at 200 RL, implying there has

Figure 9.4 Phase 4: Uplift, weathering and erosion.

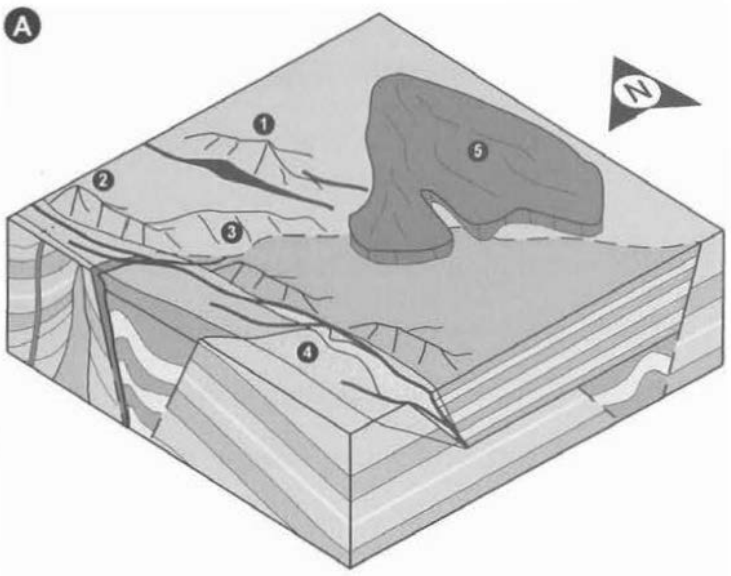

A Current land surface at Mt Muro after uplift and erosion. Silica alteration above the deposits forms resistant peaks of Mt Muro and Gunung Baruh (1) and (2), (3) and (4) QIP and kaolinite facies alteration at the deposit margins are eroded to form valleys. (5) Pho-Pleistocene basalts and late stage plugs form resistant plateaus and spires (Key to lithologies is as for Fig. 9.2, p. 308)

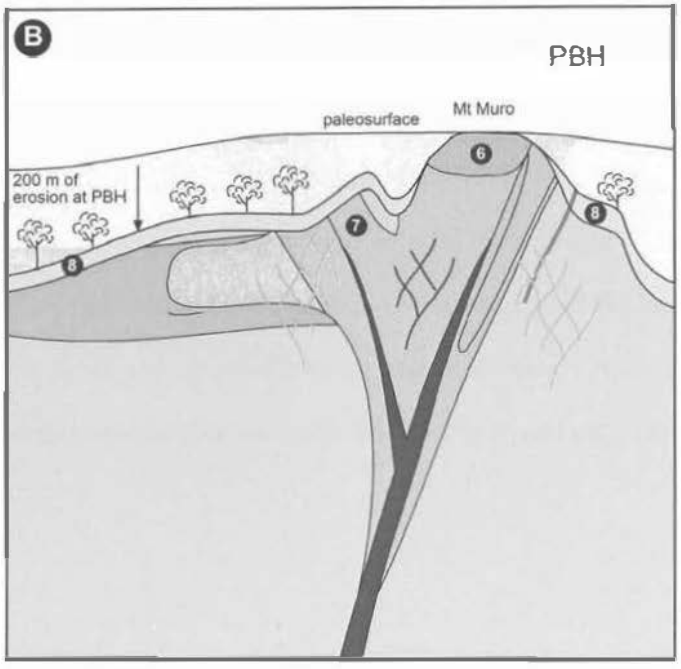

B Weathering and erosion leads to 200 m of the PBH deposit being removed. Silica facies forms the resistant peak of Mt Muro (6), while QIP alteration facies (7) alteration is weathered to form valleys at the margins to the deposits. (8) Halloysite alteration blankets the deposits and is due to the tropical weathering profile (Key to lithologies is as for Fig. 9.3, p. 310)

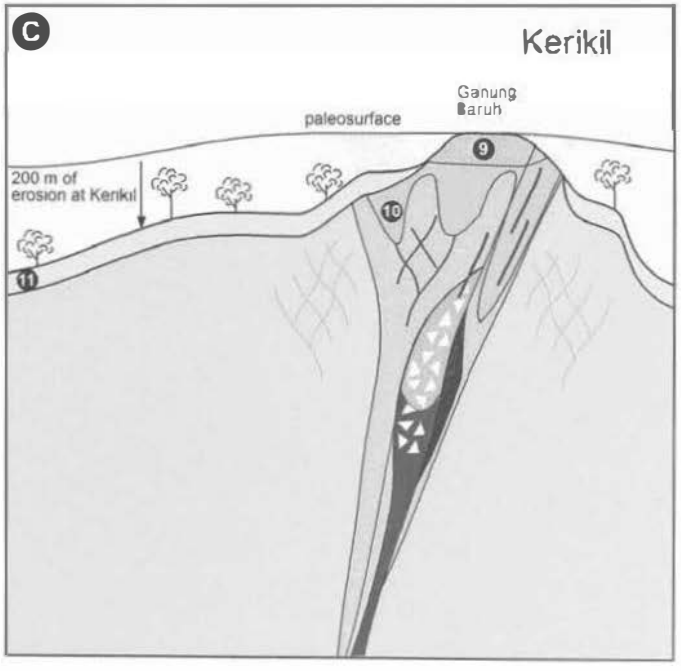

C Weathering and erosion leads to 200 m of the Kerikil deposit being removed. Silica facies forms the resistant peak of Ganung Baruh (9), while kaolinite facies flanks the silica cap (10). (11) Halloysite alteration blankets the deposits and is due to the tropical weathering profile (Key to lithologies is as for Fig. 9.3, p. 310)

been at least 200 m of erosion at Kerikil. This amount of uplift and erosion at Kerikil (200 m) is comparable with the amount of erosion and uplift at PBH (average 200 m). The Kerikil hydrothermal system represents a shallower portion of the epithermal system while PBH represents a deeper portion.

Modification of the ore deposits includes erosion of valleys through the QIP and CCA facies alteration zones adjacent to the Mt Muro deposits. However, the silicified steam-heated zones above the deposits have formed resistant silicified ridges and knobs There has also been local weathering along the vein and breccia structures. In the upper most sections of the deposits, acidic fluids created through the breakdown of pyrite in the oxide zone have leached out carbonate and volcanic clasts creating secondary permeability. This permeability has allowed the introduction of oxidized ground waters and subsequent weathering of the ore deposits to form localized manganese wad (after rhodochrosite) and secondary copper oxides (after sulfides). A thick (up to 10 m) halloysite blanket has formed over the deposits and represents a weathering profile formed in response to the wet tropical environment. Around the Mt Muro CoW, elluvial and alluvial gold deposits were formed, through the break down of exposed portions of vein and breccia body as well as gravity and traction transportation of precious metal down slopes and into streams.

CHAPTER 10

CONCLUSIONS

CHAPTER 10

CONCLUSIONS

10.1 Conclusions

The main conclusions derived from this study of the Mt Muro epithermal deposits are listed below:

- The Mt Muro Au-Ag deposits are exemplary of the low sulfidation epithermal class of ore deposit. Mineralization is hosted in veins, breccias and faults that cross-cut a predominately andesitic to basaltic sequence of volcanic and volcaniclastic host rocks of late Oligocene to Miocene age. PBH formed at deeper levels in the epithermal environment than Kerikil, which formed at relatively shallow depth.
- Twelve volcanic and sedimentary lithofacies are recognized at PBH and Kerikil. These include primary facies (coherent andesite, non-stratified monomict andesite breccia, non-stratified sediment matrix breccia, coherent basaltic andesite and coherent basalt), syn-eruptive facies (tuff and lapilli tuff), intrusive breccia facies (poorly sorted rounded exotic polymict breccia and poorly sorted rounded polymict milled breccia), and volcano-sedimentary facies (poorly sorted clast supported polymict breccia, poorly sorted muddy matrix supported polymict breccia, and stratified volcaniclastic mudstone). These lithofacies are grouped into four facies associations (based on common depositional environments) that include; a proximal slope environment, medial valley fill environment and distal basin environment, which are recognized at PBH; and a central vent facies, which occurs only at Kerikil.
- The dominant district-scale structural orientations at Mt Muro include northeast (arc parallel) and northwest (arc orthogonal) striking structures. These two orientations can be related to major island-scale tectonic features; the Kalimantan Gold Belt (Central Kalimantan Arc) and the Adang Fault zone, respectively. Rotation of Borneo and a consequent shift in the Mt Muro stress field lead to the re-alignment and distribution of stresses in these pre-existing structures and the formation of north-south to north-northwest striking dilational structures.

- The Mt Muro ore deposits are hosted by north-northwest and west-northwest striking dilational veins and breccias. PBH is characterized by north-south basin faults that were favorably aligned for dilation. At Kerikil, however, there was no pre-existing basin architecture and dilation occurred through brittle fracture of the host rocks (coherent andesites and basaltic andesites) along north-south faults. Structural bifurcations and intersections, as well as volcanic and sedimentary layering, are the main controls on the distribution of mineralization. Structures observed at Mt Muro are consistent with features expected during Reidel structural development.
- Multiple paragenetic stages were defined at PBH and Kerikil, based on mineralogical assemblages and textures. Six infill stages are recognized at PBH (stage 1: jasper, stage 2: microcrystalline quartz, stage 3: microcrystalline quartz + sulfide + sulfosalt, stage 4: quartz + sulfide, stage 5: amethyst; and stage 6 carbonate infill). Nine infill stages are recognized at Kerikil (stage 1: microcrystalline quartz; stage 2: microcrystalline quartz + sulfide + sulfosalt; stage 3: amethyst; and stage 4: carbonate; stage 5: rhodochrosite + sulfide + sulfosalt; stage 6: microcrystalline quartz + rhodochrosite; stage 7: amethyst + rhodochrosite; stage 8: quartz + sulfide; and stage 9: pyrite infill). At Kerikil, these infill stages were grouped into three periods (based on common mineralogical or textural characteristics) and include; period 1 (veins and breccias dominated by silica polymorphs), period 2 (rhodochrosite-bearing breccia infill) and period 3 (veins containing coarse-grained sulfides and pyrite). Significant differences between the two deposits include a lack of jasper at Kerikil, and the absence of rhodochrosite in direct association with ore minerals and a late pyrite stage at PBH.
- Ore mineralogy at PBH and Kerikil consists of pyrite, sphalerite, galena, chalcopyrite, silver sulfosalts, jalpaite, acanthite, covellite, native silver and electrum. Pyrite is the most common sulfide at both deposits. PBH contains relatively more sphalerite and galena compared to Kerikil, which has more abundant chalcopyrite. Electrum was noted in association with silver sulfides and sulfosalts at PBH and as inclusions in pyrite at Kerikil. Significant differences between the two deposits include the presence of Ag-tellurides at PBH, but not at Kerikil, which instead contains higher selenium concentrations (as selenium substitution in jalpaite). Ore

minerals are confined to specific paragenetic infill stages in both deposits (stages 3 and 4 at PBH; stages 2, 5 and 8 at Kerikil).

- Gangue mineralogy at PBH is dominated by silica polymorphs with carbonate occurring only in the latest infill stage. At Kerikil, silica polymorphs dominate early in the paragenesis and rhodochrosite becomes more prominent in later infill stages. A common feature of the two deposits is a transition from fine-grained, silica-dominated gangue minerals in early infill stages to significantly coarser-grained infill (with carbonate) in the later paragenetic stages. This suggests a transition from silica-saturated fluids and a rapid rate of precipitation (likely in response to boiling conditions), to a slower rate of mineral deposition (likely in response to cooling). The switch to coarser-grained crystals generally marks the end of ore deposition and, by association, the cessation of boiling.
- On a regional-scale, base metal anomalism in surface samples and soils is centered on two hydrothermal systems at Mt Muro and Ganung Baruh. On a deposit-scale, assay data indicate that precious metal mineralization is confined to north-northwest and north-south striking dilation structures. Metal distribution is systematically zoned at PBH, from base metals at depth to precious metals at shallow levels. In contrast, base and precious metals occur at approximately the same level at Kerikil. In both deposits, metals are confined to high permeability, fluid flow pathways such as pre-existing basin faults, bifurcations in the deposit structure, structural intersections and volcanic layer boundaries. Metal ratios indicate that ore-bearing fluids generally flowed upwards along the north-northwest striking dilation structures and outwards from the intersection of northwest striking structures at both PBH and Kerikil.
- Alteration on a regional-scale is recognized as two large areas of magnetite destruction and clay alteration centered on Mt Muro and Ganung Baruh. On a deposit-scale, alteration mineralogy at PBH and Kerikil is dominated by quartz, chlorite, illite, sericite, phengite, carbonate, pyrite, adularia, albite, kaolinite, halloysite and epidote. In general, silica is the most abundant alteration mineral and pyrite, although not abundant, is the most widespread. Alteration mineral assemblages indicate that the mineralizing fluids at PBH and Kerikil were of

moderate to high temperature (180° to 250°C) and ranged from acidic to near neutral pH. A late-stage kaolinite overprint at Kerikil is related to considerably cooler (>150 to <200°C) acid sulfate waters.

- Alteration facies at PBH and Kerikil are defined on the basis of mineral assemblages. These facies include the CCA alteration facies (chlorite + carbonate + epidote + pyrite), the SPA alteration facies (quartz + sericite + phengite + adularia + pyrite), the QIP alteration facies (quartz + illite + pyrite), the kaolinite alteration facies (kaolinite dominant), the silica alteration facies (silica dominant), and halloysite alteration facies (halloysite dominant). All six alteration facies were recognized at PBH, but the SPA facies is not recognized at Kerikil (due to lack of basin sediments that host the alteration).
- Alteration at PBH is zoned both laterally and vertically. QIP alteration facies occurs proximal to the deposit and is well developed in the hanging wall. The QIP facies is flanked by CCA alteration. The SPA alteration facies is lithogically controlled and occurs in tuffs and lapilli tuffs. Silica alteration facies forms resistant ridges and peaks above the deposit. Kaolinite alteration is confined to footwall fault gouge. Halloysite alteration occurs at or near the surface and is most likely related to a weathering profile. At Kerikil, alteration is also zoned but is complicated by an extensive, late-stage kaolinite overprint. QIP alteration occurs proximal to the veins and is flanked by the CCA facies. Kaolinite alteration overprints both these facies at higher elevations in the deposit. Silica facies alteration is responsible for the resistant peak of Ganung Baruh and halloysite alteration is again most likely a weathering feature.
- Whole rock data indicate geochemical variations between different alteration facies and with increasing alteration intensity (measured by the Alteration Index; Ishikawa et al., 1976). All alteration types at PBH and Kerikil are depleted in Na_2O and CaO relative to unaltered host rocks, and enriched in K_2O, Fe_2O_3 and S. MnO and MgO depletion at Kerikil is related to destruction of mafic minerals in the volcanic host rocks. At both PBH and Kerikil, Nb, Y, and V remain constant across alteration facies and are inferred to be relatively immobile under the hydrothermal conditions at Mt Muro. Ore-related elements all increase with increasing Alteration Index,

reflecting greater interaction of the host rocks with the mineralizing fluid closer to the mineralized zones. Hg and As values are highest in the upper alteration zones of both deposits.

- Fluid inclusion measurements for the Mt Muro deposits were reported previously in Simmons and Browne (1990). Data suggest that the ore fluid at PBH was relatively high temperature (238° to 262°C), moderately saline (less than 3.2 eq. wt % NaCl) and precipitated at depths of 400 m below the water table. At Kerikil, mineralizing fluids were of slightly lower temperature (207° to 253°C), slightly higher salinity (less than 4.1 eq. wt % NaCl), and precipitated at depths of 225 and 400 m below the water table. Fluid inclusion studies report characteristics consistent with sealing of the hydrothermal system at Kerikil (Simmons and Browne, 1990).
- Sulfur and carbon isotope data suggest a magmatic source of sulfur and carbon. However, there is a trend towards higher values $\delta^{13}C$ values with progressively later infill stages at Kerikil, suggesting the influence of a higher $\delta^{13}C$ source. $\delta^{13}C$ values from PBH and Kerikil have similar values to CO_2 and HCO_3^- taken from modern geysers and are unlike carbon derived from carbonate host rocks. Data are consistent with $\delta^{13}C$ and $\delta^{18}O$ derivation from HCO_3^-, rather than H_2CO_3, and were likely produced from boiling processes.
- Oxygen isotope data for quartz and carbonate infill stages at PBH show a trend towards higher values with progressively younger infill stages. At Kerikil, $\delta^{18}O$ values are consistent across infill stages, except for the last stage, where there is a trend towards higher values. This trend likely reflects a temperature change or different $\delta^{18}O$ source (i.e., the incursion of surficial meteoric waters during the waning stages of the hydrothermal system). Calculated $\delta^{18}O$ values for fluid in equilibrium with quartz from both deposits are close to 0‰ and are consistent with a meteoric water source. Oxygen isotope data for whole rock samples of alteration facies at PBH show a correlation between lower $\delta^{18}O$ values with proximity to mineralization. In contrast, $\delta^{18}O$ values are relatively consistent across different alteration facies at Kerikil. Both deposits have a late-stage, high $\delta^{18}O$ overprint associated with kaolinite and/or halloysite alteration. Average $\delta^{18}O$ values for all alteration facies in both deposits are similar those for unaltered volcanic host rocks

(7 to 9‰), suggesting that the initial alteration fluids were equilibrated with the host rock (indicating high water to rock ratios).

- The major controls on ore deposition for the Mt Muro deposits on a regional scale include;
  - A heat source from a volcanic pile or magma at depth to drive hydrothermal convection;
  - Dilational structures as a focus for hydrothermal fluids circulating within the regional convection cell.
- At Mt Muro, the heat source is provided by magmatism coincident with the Central Kalimantan Arc, and focusing structures are provided by dilational structures that formed in response to regional strike slip faulting (resulting from structural re-organization due to the island scale rotation of Borneo).
- On a deposit-scale, critical features for ore deposition at PBH and Kerikil include;
  - Structures that allow high flow rates for the mineralizing fluid;
  - Subsequent dilation of structures to allow depressurization, boiling and/or mixing of the mineralizing fluid, thus inducing mineral precipitation.
- Differences in the host lithologies (and thus rheologies) and relative depth of formation of the two deposits led to significantly different structural regimes into which ore and alteration fluids were emplaced. The textural, geochemical, and mineralogical signatures of the two deposits reflect this variability, and are represented by the two 'end-member' deposit styles of PBH and Kerikil. The relative importance of boiling and/or mixing as efficient mechanisms for metal precipitation in the two deposits reflect fundamental geological and structural controls on alteration and epithermal mineralization.

10.2 Implications for exploration

The final aim of this research project was to determine specific characteristics of the Kerikil and PBH deposits that would aid in the search and discovery of new mineralized zones in the Mt Muro district. Exploration criteria are thus outlined in the following section by examining the footprint of the mineralizing system on a regional scale (Fig. 10.1) and volcanological, structural, mineralogical, metal zoning and alteration features of

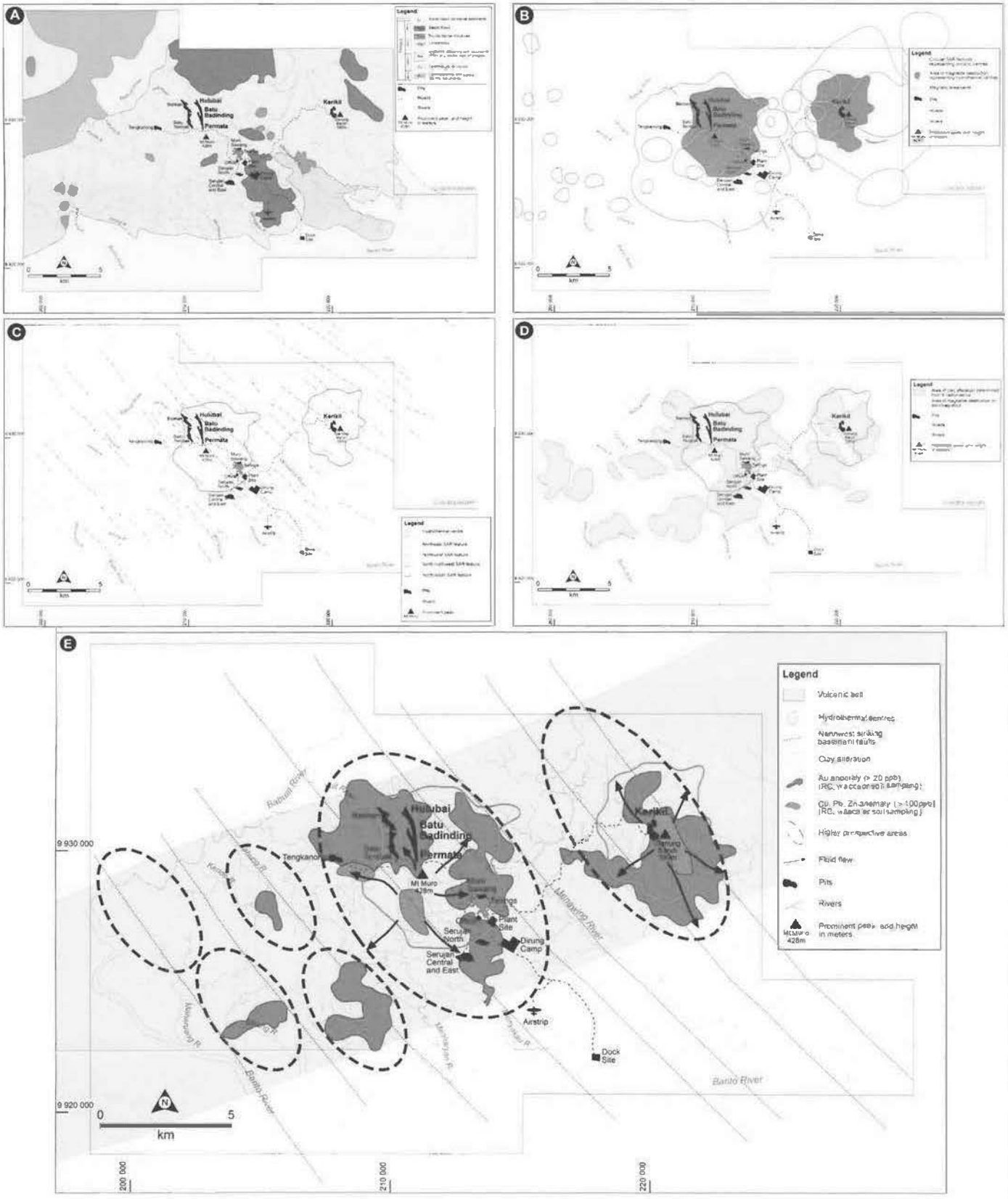

Figure 10.1 CoW maps showing footprint of Mt Muro mineralization and prospective regions.

A Mt Muro mineralization lies within a belt of northeast-trending andesitic to basaltic and-site volcanic rocks.

B Numerous circular features can be seen on SAR imagery and are thought to represent volcanic centres, intrusions and plugs. The circular features have a roughly northeast trend. Two large areas of magnetic destruction are situated in the centres of the regional circular features which represent the centres of two former hydrothermal cells. The Mt Muro epithermal deposits sit within the bounds of the two largest circular SAR features and magnetic low areas.

C Several sets of lineaments can be seen in SAR and are related to northeast (arc parallel) striking structures, northwest (basement) striking structures, and north-northwest and west-northwest trending dilation structures. The deposits strike north-northwest and west-northwest and are typically situated at the junctions of northwest striking structures.

D The deposits are associated with large areas of clay alteration. The clay alterations is controlled by northeast and northwest structures.

E Ideal sites for mineral exploration are where northwest striking basement structures cut across the northeast trending volcanic belt. Fluid has flowed upward and outward away from the centres of two former hydrothermal cells. Base metal zonation shows the centre of these cells, while gold anomalism is situated around the margins of the cells.

PBH and Kerikil on a deposit-scale (Figs. 10.2 and 10.3). Although epithermal mineralization was the main focus of this study, there is considerable scope for other mineralization styles to be targeted at Mt Muro, as outlined in Figure 10.2.

Volcanological features: The stratigraphic framework outlined in this study provides a solid background and reference point for further mineral exploration. On a regional-scale, it is important to identify the position of the paleo-arc as the source of heat for large, potentially fertile, hydrothermal convection cells. These hydrothermal cells can be recognized as areas of magnetite destruction (Fig. 10.1 B). Similarly, paleo-volcanic centres can be identified by geological mapping and as circular regions on SAR imagery (Fig. 10.1 A and B). Within this broad geological framework, extensional regimes with favorably aligned (for dilation), pre-existing graben structures represent potential hosts for PBH vein style deposits. The recognition of these pre-existing structures and basinal environments can be achieved by detailed lithological mapping. For example, basin bounding faults at PBH are defined by the extents and controls on the medial valley and distal basin fill environment facies associations.

Structural features: On a regional-scale, intersections of northwest striking structures with the northeast trending Kalimantan Gold Belt are important controls on mineralization and represent favorable exploration targets (Fig. 10.1 C). These features can be recognized on the CoW-scale by the presence of northeast striking dikes (coincident with the Kalimantan Gold Belt) and northwest striking dikes (coincident with the northwest basement structures). The presence of hydrothermal cells associated with the intersection of northwest structures and northeast trending volcanic arc can be delineated (using geophysical imagery) as magnetic lows and K-Th highs (Fig. 10.1 D and E). In addition to large hydrothermal circulation cells, however, dilational structures are required to focus the mineralizing fluids. Favorable dilational structural settings can occur along northwest striking structures as flexures and jogs or compressional brecciated jogs. Intersections of northwest striking structures with geological boundaries of high competency contrast may also provide favorable dilational sites.

Geophysical surveys are useful for identifying potential ore-related structures. Northwest striking structures associated with mineralization can be defined by magnetic susceptibility highs and lows, depending on the presence of basaltic andesite dikes or

magnetite destruction. Magnetic susceptibility highs are typically related to post mineral basaltic dikes. Northwest striking structures may also be distinguished using SAR or aerial photos to define topographic highs and lows. This will depend on whether there is silicification or destructive alteration associated with the structure. Favorable target areas also include zones where northwest striking structures have been covered (by later volcanic, volcanoclastic and sedimentary rocks) and subsequently reactivated to produce tensional fractures, as per the Riedel clay box model (e.g., Figure 3.8). This produces north-south high angle structures that are typically silicified and resistant with high topographic relief. These structures rarely have a strong magnetic signature but are discernable on SAR and topographic maps. Mineralization can thus be targeted using the intersection of magnetic imagery highs (northwest structures) with areas of high topographic relief from SAR or aerial photos (north-south and north-northwest striking structures). In the northwestern part of the COW, northwest striking structures extend into the limestone basement and may be excellent sites for carbonate replacement style ore bodies (Figure 10.2).

The en echelon style of structural repetition associated with Riedel fracture sets indicates that there may be further north-south striking, parallel vein style deposits to the west and east of PBH and Bantian-Batu Tembak (BBT). An ideal site to test this would be to the west of BBT where north-south striking structures are developed above major northwest trending basement structures.

There is further scope for "blind" or hidden ore bodies at Mt Muro beneath the impermeable cap rocks. Contrasting lithologies in the stratovolcano setting can exert significant influence on the hydrology of the hydrothermal system, and mineralizing fluids could easily be trapped beneath impermeable cap rocks. "Blind" deposits may be targeted using the structural criteria (intersections of northwest and north-south striking structures) outlined above, in addition to metal zonation and ratio studies to track northwest striking structures and boiling levels.

Mineralogical features: The PBH and Kerikil style deposits are characterized by high rates of focused fluid flow that are recognized by the presence of large amounts of fine-grained banded silica and, in particular, microcrystalline quartz. Bonanza grades are commonly associated with boiling zones (Fig. 10.3). These zones can be identified by

Figure 10.2 Block model showing possible mineralization styles at Mt Muro

Schematic block diagram showing the relative location of the Mt Muro deposits within the structural and geological framework outlined in this study and the range of mineralization (colored blue) possibilities at Mt Muro.

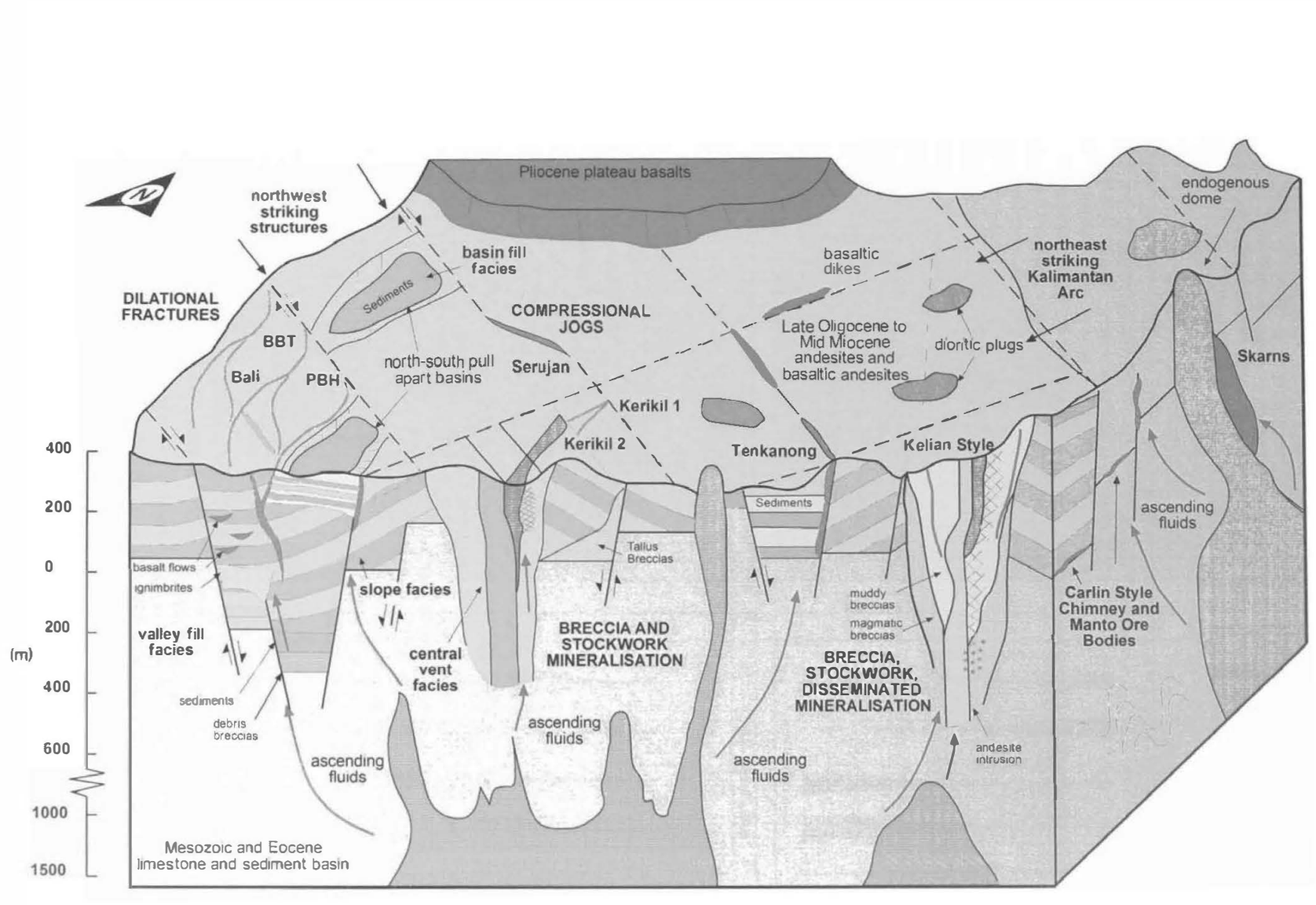

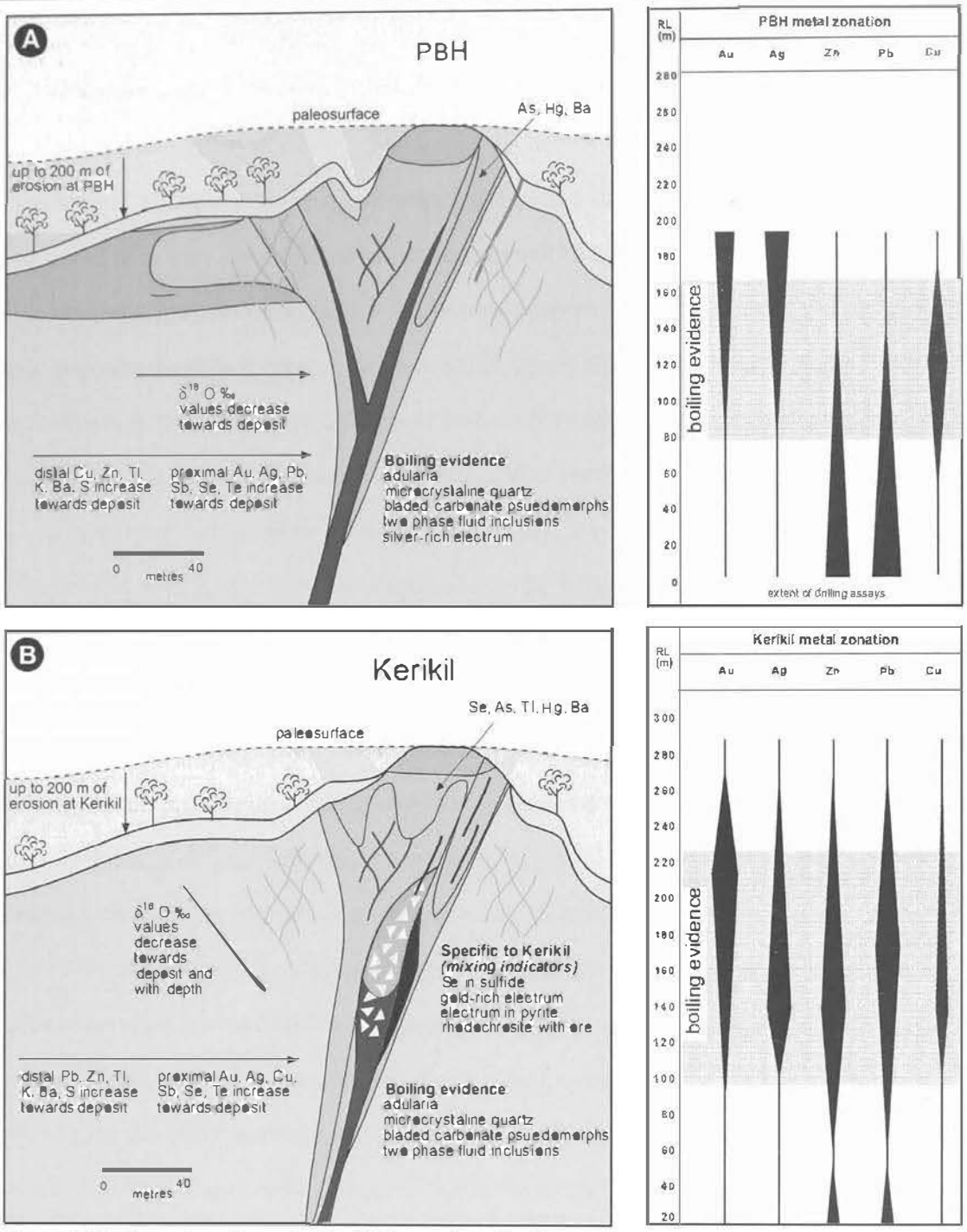

Figure 10.3 Deposit-scale vectors to Mt Muro mineralization

A PBH-style mineralization showing deposit scale mineralization features. Alteration is zoned from distal CCA and SPA facies alteration to proximal QIP facies alteration. Silica and Kaolinite alteration facies is seen at shallow levels and halloysite alteration facies blankets the deposit. $\delta^{18}O$ values become lighter towards mineralization. Precious metals are deposited at and above the zone of boiling, base metals are deposited below. Whole rock geochemistry shows increases in Au, Ag, Pb, Sb, Se and Te at the immediate margins to the deposit and increases in Cu, Zn, Tl, K, Ba and S further away from the deposit. Carbonate veins are seen in the peripheries to the deposit in the hanging-wall and footwall. Surface alteration is enriched in As, Hg and Ba. Silica alteration forms prominent ridges and peaks. (Key as per Fig. 9.3 on page 311)

B Kerikil-style mineralization showing deposit scale mineralization features. Alteration is zoned from distal CCA facies alteration to proximal QIP facies alteration. Silica and Kaolinite alteration facies is seen at shallow levels and overprints the QIP facies alteration. Halloysite alteration facies blankets the deposit. $\delta^{18}O$ values become lower with depth from surface and towards mineralization. Precious metals and base metals are deposited together in the zone of boiling and/or mixing. Whole rock geochemistry shows increases in Au, Ag, Cu, Sb, Se and Te at the immediate margins to the deposit and increases in Pb, Zn, Tl, K, Ba and S further away from the deposit. Carbonate veins are seen in the peripheries to the deposit in the hanging-wall and footwall. Surface alteration is enriched in Se, As, Tl, Hg and Ba. Silica alteration forms prominent ridges and peaks. (Key as per Fig. 9.3 on page 311)

gangue mineralogy and textural characteristics such as microcrystalline quartz, adularia and/or mineral pseudomorphs after bladed calcite (Fig. 10.3). Other mineralogical features may be used as a guide to relative position in the hydrothermal system. For example, rhodochrosite occurs in the upper portions of the deposits and may or may not be associated with ore. The dominant ore minerals will vary between the PBH and Kerikil style deposits. Sphalerite and galena are generally common in the deeper parts of PBH style deposits. Se substitution in sulfide is common in Kerikil style deposits. Electrum is typically silver-rich in PBH style deposits and silver resides in a range of silver sulfosalts and sulfides. At Kerikil, electrum is gold-rich and commonly occurs as inclusions in pyrite.

Metal zonation features: In general, base and precious metals in the Mt Muro deposits are vertically zoned, with precious metals above the boiling zone and base metals increasing with depth (Fig. 10.3). This is important when considering the vertical extent of the hydrothermal system and the potential for mineralized zones at depth. Results from this study suggest that extensions to the PBH and Kerikil ore deposits below 0 RL are unlikely. Metal ratio studies indicate that major northwest striking structures are important fluid conduits, and the intersection of north-northwest striking structures and northwest striking structures are important sites of ore deposition.

Alteration vectors: The PBH and Kerikil deposits are associated with narrow alteration halos. Alteration is zoned with QIP, silica and kaolinite alteration facies occurring within tens of meters of the deposit; and SPA and CCA alteration facies extending up to tens to 100's of meters away from the deposit (Fig. 10.3). On a district-scale, silica alteration can be recognized as ridges and knobs, and the flanking QIP and SPA alteration facies are often weathered to form valleys. CCA alteration, which represents the recharge area of the hydrothermal system, can be determined on magnetic imagery (as a magnetite destruction halo) or radiometrics (as a regional K-Th anomaly) and may extend for kilometers from the vein system (Fig. 10.1 D). Deposits of Kerikil-style would be overprinted by the late collapse and brecciation of the hydrothermal system, giving rise to extensive kaolinite alteration (Fig. 10.3 B).

Geochemical vectors to ore are summarized on Figure 10.3. In general, K_2O, Fe_2O, S, Au, Ag, Pb, Zn, Cd, Sb, As, Tl, Se, Te, Hg, Mo, Bi, Rb and Ba increase with proximity to the deposits. Elevated Au, Ag, Se and Te also occur proximal (within 10 m of ore) to

the vein system, whereas elevated Cu, Zn, Pb, Tl, K Ba and S occur outwards of the precious metal anomalies (e.g., within 40 m of ore at PBH and within 20 m at Kerikil). NaO_2, CaO, MgO and MnO are progressively depleted with proximity to the deposits. High level kaolinite alteration is associated with elevated As, Tl, Hg, Ba and Se values.

10.3 Future research directions

The geological framework determined in this project from comprehensive studies of the volcanic architecture, structure, mineralization, and alteration caharacteristics of the Mt Muro deposits provides a strong base for further research. Future research directions could include;

- Age dating of Mt Muro volcanics. This would not only help to place Mt Muro in the regional geological and structural framework, but also constrain the age of volcanism relevant to mineralization. Furthermore, dating of the mineralization could be carried out on adularia, while sericite could be used for dating the alteration facies. This would help to constrain the timing of mineralization relative to magmatism.
- Evaluation of regional metallogenesis. Comparison of the Mt Muro deposits to other epithermal systems in the Kalimantan Gold Belt (e.g., Marsupa Ria and Kelian) could identify common features and aid in the exploration for similar deposits within the belt.
- A detailed examination of selenium substitution in sulfides at Kerikil. This data could be used as comparison to other Se-rich epithermal deposits to determine common genetic links. Selenium substitution can be attributed to mixing with oxidized ground waters and thus may distinguish epithermal deposits in which mixing of oxidized ground waters has been a factor in ore deposition.
- A detailed study of the relative trace metal abundances in pyrite (using laser ablation techniques). Of particular interest is the residency and distribution of Tl within pyrite as an indicator of low temperature regions above a previously boiling hydrothermal system.
- Detailed mineralogical and geochemical studies of silver minerals in the Mt

Muro deposits. Based on initial results from this study, there is scope for several new silver minerals to be discovered.

- Further research into the significance and genesis of rhodochrosite in low sulfidation epithermal deposits (such as Kerikil). Rhodochrosite occurs in selected epithermal systems, and may indicate the presence of steam-produced bicarbonate waters. The occurrence of rhodochrosite may distinguish epithermal deposits where mixing of bicarbonate waters has been a factor in ore deposition.
- Detailed studies of chlorite mineral chemistry. In particular, variation of Fe and Mg ratios in chlorite, either laterally or vertically within the deposits, may be used as a vector to mineralization.
- Additional fluid inclusion analyses. The data currently available is based only on limited paragenetic stages within the Mt Muro deposits. Further studies may be able to ascertain the pressure and temperature conditions in the fine-grained pre- and syn-mineralization stages at PBH and Kerikil, in order to better constrain the physico-chemical conditions of ore deposition.

References

REFERENCES

Abidin, H. Z., 1996, The tectonic history and mineral deposits of the east-central Kalimantan volcanic belt, Indonesia: A comparative study of the Kelian, Muyup and Masupa Ria gold deposits: Unpub. PhD thesis, The University of Adelaide. p. 230.

Albinson F, T., Clark, K. F., and Salas P, G. A., 1988, Geologic reconstruction of paleosurfaces in the Sombrerete, Colorada, and Fresnillo districts, Zacatecas State, Mexico: Economic Geology, v. 83, p. 1647-1667.

Barnes, H. L., 1979, Solubilities of ore minerals, in Barnes, H. L., ed.: New York, John Wiley & Sons. p. 971.

Barnes, H. L., Adams, S. S., and Rose, A. W., 1978, Status of research on diagenetic ore-forming processes, Abstracts with Programs - Geological Society of America, 10: Boulder, Geological Society of America (GSA), p. 363.

Bastin, E. S., and Hill, J. M., 1917, Economic Geology of Gilpin County and Adjacent Parts of Clear Creek and Boulder counties, Colorado: Reston, U. S. Geological Survey. p. 1-65

Bellon, H., Rangin, C., Silver, E. A., von Breymann, M. T., Berner, U., Bertrand, P., Betzler, C., Brass, G. W., Hsue, V., Huang, Z., Jarrard, R. D., Lewis, S. D., Linsley, B. K., Merrill, D. L., Mueller, C. M., Nederbragt, A. J., Nichols, G. J., Pubellier, M., Sajona, F. G., Scherer, R. P., Sheu, D. D., Shibuya, H., Shyu, J.-P., Smith, R. B., Smith, T., Solidum, R. U., Spadea, P., and Tannant, D. D., 1991, Geochemistry and isotopic dating of Cenozoic volcanic arc sequences around the Celebes and Sulu seas: Proceedings of the Ocean Drilling Program, Scientific Results, v. 124, p. 321-338.

Bente, K., and Doering, T., 1993, Solid-state diffusion in sphalerites; an experimental verification of the "chalcopyrite disease": European Journal of Mineralogy, v. 5, p. 465-478.

Bente, K., and Doering, T., 1995, Experimental studies on the solid state diffusion of Cu + In in ZnS and on "disease", DIS (Diffusion Induced Segregations), in sphalerite and their geological applications: Mineralogy and Petrology, v. 53, p. 285-305.

Berger, B. R., and Henley, R. W., 1989, Advances in the understanding of epithermal gold-silver deposits, with special reference to the Western United States: Economic Geology Monographs, v. 6, p. 405-423.

Bowen, G. J., and Wilkinson, B., 2002, Spatial distribution of $\delta^{18}O$ in meteoric precipitation: Geology, v. 30 (4), p. 315-318.

Brathwaite, R. L., and Faure, K., 2002, The Waihi epithermal gold-silver-base metal sulfide-quartz vein system, New Zealand; temperature and salinity controls on electrum and sulfide deposition: Economic Geology, v. 97, p. 269-290.

Bret, L., Fevre, Y., Join, J.-L., Robineau, B., and Bachelery, P., 2003, Deposits related to degradation processes on Piton des Neiges Volcano (Reunion Island); overview and geological hazard, in Rymer, H., and Williams-Jones, G., eds., Journal of Volcanology and Geothermal Research, 123: Amsterdam, Elsevier, p. 25-41.

Broderick, T. M., 1929, Zoning in Michigan copper deposits and its significance: Economic Geology, v. 24, p. 149-162.

Brown, W. H., 1935, Quantitative study of ore zoning, Austinville Mine, Wythe County, Virginia: Economic Geology and the Bulletin of the Society of Economic Geologists, v. 30, p. 425-433.

Brown, S. R., and Bruhn, R. L., 1996, Formation of voids and veins during faulting: Journal of Structural Geology, v. 18, p. 657-671.

Browne, P. R. L., 1978, Hydrothermal alteration in active geothermal fields: Annual Review of Earth and Planetary Sciences, v. 6, p. 229-250.

Browne, P. R. L., and Ellis, A. J., 1970, The Ohaki-Broadlands hydrothermal area, New Zealand; mineralogy and related geochemistry: American Journal of Science, v. 269, p. 97-131.

Bryner, L., 1962, Breccia and pebble columns associated with epigenetic ore deposits: Economic Geology, v. 57, p. 114-115.

Buchanan, L. J., 1981, Precious metal deposits associated with volcanic environments in the Southwest, in Dickinson, W. R., and Payne, W. D., eds., Arizona Geological Society Digest, vol.14: Tucson, Arizona Geological Society, p. 237-262.

Busby-Spera, C. J., and White, J. D. L., 1987, Variation in peperite textures associated with differing host-sediment properties: Bulletin of Volcanology, v. 49, p. 765-776.

Camana, G., Chateigner, D., Zucall, M., and Artioli, G., 2002, The grid-work texture of authigenic microcrystalline quartz in siliceous crust-type (SCT) mineralized horizons: American Mineralogist, v. 87, p. 1128-1138.

Camprubí, A., Canals, A., Cardellach, E., Prol-Ledesma, R., and Rivera, R., 2001, The La Guitarra Ag-Au low-sulfidation epithermal deposit, Temascaltepec District, Mexico:

vein structure, mineralogy and sulfide sulfosalt chemistry in Albinson, T., and Nelson, C. E., New Mines and Discoveries in Mexico and Central America: Society of Economic Geologists Special Publication v. 8, p. 133-158.

Campbell, A. R., and Larson, P. B., 1998, Introduction to stable isotope applications in hydrothermal systems: Reviews in Economic Geology, v. 10, p. 173-193.

Carlile, J. C., and Mitchell, A. H. G., 1994, Magmatic arcs and associated gold and copper mineralization in Indonesia: Journal of Geochemical Exploration, v. 50, p. 91-142.

Cas, R. A. F., and Wright, J. V., 1987, Volcanic successions: modern and ancient. A geological approach to processes, products and successions, Chapman & Hall, London, p. 528.

Clayton, R.N. 1992, Oxygen isotopes in geothermometry: 29th International Geological Congress Abstracts, v. 29, p. 592.

Clayton, R. N., and Mayeda, T. K., 1963, The use of bromine pentafluoride in the extraction of oxygen from oxides and silicates for isotopic analysis: Geochimica et Cosmochimica Acta, v. 27, p. 43-52.

Cloke, I. R., Moss, S. J., and Craig, J., 1999, Structural controls on the evolution of the Kutai Basin, East Kalimantan, in Lambiase, J. J., Morley, C. K., Ronghe, S. S., Simmons, M. D., Van Rensbergen, P., and Barber, A. J., eds., Journal of Asian Earth Sciences, 17: Oxford, Pergamon, p. 137-156.

Cooke, D. R., and Bloom, M. S., 1990, Epithermal and subjacent porphyry mineralization, Acupan, Baguio District, Philippines; a fluid-inclusion and paragenetic study: Journal of Geochemical Exploration, v. 35, p. 297-340.

Cooke, D. R., and McPhail, D. C., 2001, Epithermal Au-Ag-Te mineralization, Acupan, Baguio District, Philippines; numerical simulations of mineral deposition: Economic Geology, v. 96, p. 109-131.

Cooke, D. R., and Simmons, S. F., 2000, Characteristics and genesis of epithermal gold deposits: Reviews in Economic Geology, v. 13, p. 221-244.

Corbett, J. G., and Leach, T. M., 1998, Southwest Pacific Rim gold-copper systems: Structure, alteration, mineralisation: Society of Economic Geologists Special Publication, v. 6, p. 237.

Cox, K. G., Bell, B. G. and Pankhurst, R.J., 1979, The interpretation of igneous rocks. Unwin Hyman, London, p. 450.

Crerar, D. A., Cormick, R. K., and Barnes, H. L., 1980, Geochemistry of manganese; an overview, in Varentsov, I. M., and Grasselly, G., eds.: Stuttgart, E. Schweizerbart'sche Verlagsbuchhandlung.

Cross, W., 1896, Geology of Silver Cliff and the Rosita Hills, Colorado: U.S. Geology Survey 17th Annual Report, Part II, p. 263-403.

Daly, M. C., Cooper, M. A., Wilson, I., Smith, D. G., and Hooper, B. G. D., 1991, Cenozoic plate tectonics and basin evolution in Indonesia: Marine and Petroleum Geology, v. 8, p. 2-21.

Davies, A. G. S., Cooke, D. R., and Gemmell, J. B., 1999, Characteristics, timing and formation of diatreme breccias at the Kelian gold deposit, East Kalimantan, Indonesia: PACRIM, 1999, p. 718.

Davies, A. G. S., Cooke, D. R., and Gemmell, J. B., 2000, Overlaps between phreatic and phreatomagmatic brecciation - implications for the development of hydrothermal systems. An example from the Kelian gold deposit, East Kalimantan, Indonesia: 15th Australian Geological Convention, University of Technology, Sydney, Australia, July 3-7, 2000, p. 119.

Deer, W.A. Howie, R.A., and Zussman, J., 1992, An introduction to the rock-forming minerals, Longman Scientific and Technical, 696 p.

Dennen, W. H., and Puckett, A. M., 1972, On the chemistry and color of amethyst: The Canadian Mineralogist, v. 11, p. 448-456.

Dong, G., and Morrison, G. W., 1995, Adularia in epithermal veins, Queensland; morphology, structural state and origin: Mineralium Deposita, v. 30, p. 11-19.

Dong, G., Morrison, G., and Jaireth, S., 1995, Quartz textures in epithermal veins, Queensland; classification, origin and implication: Economic Geology, v. 90, p. 1841-1856.

Doutch, H. F., 1992, Aspects of the structural histories of the Tertiary sedimentary basins of East, Central and West Kalimantan and their margins: Journal of Australian Geology and Geophysics, v. 13, p. 237-250.

Dowling, K., and Morrison, G., 1989, Application of quartz textures to the classification of gold deposits using North Queensland examples: Economic Geology Monographs, v. 6, p. 342-355.

Einaudi, R. H., Hedenquist, J. W., and Inan E. E., 2003, Sulfidation of fluids in active and extinct hydrothermal systems: transitions from porphyry to epithermal environments in Simmons, S.F., and Graham, I., ed., Volcanic, geothermal, and ore forming fluids: Society of Economic Geologists Special Publication, no. 10, p. 315-343.

Emmons, S.F., 1896, The mines of Custer County, Colorado: U.S. Geology Survey 17th Annual Report, Part II, p. 405-472.

Ewers, G. R., and Keays, R. R., 1977, Volatile and precious metal zoning in the Broadlands geothermal field, New Zealand: Economic Geology, v. 72, p. 1337-1354.

Fellows, M. L., and Hammond, J. M., 1990, Wirralie gold deposit, Queensland, in Hughes, F.E., ed. Geology of the mineral deposits of Papua New Guinea: Australasian Institute of Mining and Metallurgy Monograph 14, p. 1489-1492

Field, C. W., and Fifarek, R. H., 1985, Light stable-isotopes systematics in the epithermal environment: Reviews in Economic Geology, v. 2, p. 99-128.

Fink, J. H., and Manley, C. R., 1987, Origin of pumiceous and glassy textures in rhyolite flows and domes, in Fink, J. H., ed., Special Paper - Geological Society of America, vol.212: Boulder, Geological Society of America (GSA), p. 77-88.

Fisher, R. V., 1960, Classification of volcanic breccias: Geological Society of America Bulletin, v. 71, p. 973-981.

Fisher, R. V., 1961, Proposed classification of volcaniclastic sediments and rocks: Geological Society of America Bulletin, v. 72, p. 1409-1414.

Fournier, R. O., 1985a, Silica minerals as indicators of conditions during gold deposition, in Tooker, E. W., ed., U. S. Geological Survey Bulletin, Report: B 1646: Reston, U. S. Geological Survey, p. 15-26.

Fournier, R. O., 1985b, The behavior of silica in hydrothermal solutions: Reviews in Economic Geology, v. 2, p. 45-61.

Fuller, M., Ali, J. R., Moss, S. J., Frost, G. M., Richter, B., and Mahfi, A., 1999, Paleomagnetism of Borneo, in Lambiase, J. J., Morley, C. K., Ronghe, S. S., Simmons, M. D., Van Rensbergen, P., and Barber, A. J., eds., Journal of Asian Earth Sciences, 17: Oxford, Pergamon, p. 3-24.

Gammons, C. H. and Seward, T. M., 1996, Stability of Mn(II) chloride complexes from 25 to 300°C: Geochemica et Cosmochimica Acta, v. 60, p. 4295-4311.

Gammons, C.H., and Williams-Jones, A.E., 1995, Hydrothermal geochemistry of electrum: thermodynamic constraints: Economic Geology, v. 90, 420-432.

Gemmell, J. B. 2001a, Hydrothermal alteration associated with the Gosawong low sulfidation epithermal Au-Ag vein deposit, Indonesia: ARC-AMIRA P588 Report 3, June 2001, p. 1-43.

Gemmell, J. B. 2001b, Hydrothermal alteration associated with the Gosawong low sulfidation epithermal Au-Ag vein deposit, Indonesia: ARC-AMIRA P588 Report 4, December 2001, p. 1-34.

Gemmell, J. B., and Large, R. R., 1992, Stringer system and alteration zones underlying the Hellyer volcanogenic massive sulfide deposit, Tasmania, Australia: Economic Geology , v. 87, p. 620-649.

Gemmell, J. B., Simmons, S. F., and Zantop, H., 1988, The Santo Nino silver-lead-zinc vein, Fresnillo District, Zacatecas, Mexico: Part I. Structure, vein stratigraphy and mineralogy: Economic Geology, v. 83, p. 1598-1618.

Giggenbach, W. F., 1981, Geothermal mineral equilibria: Geochimica et Cosmochimica Acta, v. 45, p. 393-410.

Giggenbach, W. F., 1987, Redox processes governing the chemistry of fumarolic gas discharges from White Island, New Zealand: Applied Geochemistry, v. 2, p. 143-161.

Giggenbach, W. F., 1988, Geothermal solute equilibria, derivation of Na-K-Mg-Ca geoindicators: Geochimica et Cosmochimica Acta, v. 52, p. 2749-2765.

Giggenbach, W. F., 1988, The interplay of magmatic and hydrothermal processes in the formation of volcanic and geothermal fluid discharges: Tokyo, National Institute of Resource Advancement. p.25-32

Goodell, P. C., and Petersen, U., 1974, Julcani Mining District, Peru: A Study of Metal Ratios: Economic Geology, v. 69, p. 347-361.

Gustafson, L. B., and Hunt, J. P., 1975, The porphyry copper deposit at El Salvador, Chile: Economic Geology and the Bulletin of the Society of Economic Geologists, v. 70, p. 857-912.

Haas, J. L., Jr., 1971, The effect of salinity on the maximum thermal gradient of a hydrothermal system at hydrostatic pressure: Economic Geology, v. 66, p. 940-946.

Hall, R., 1996, Reconstructing Cenozoic SE Asia, in Hall, R., and Blundell, D. J., eds., Geological Society Special Publications, vol.106: London, Geological Society of London, p. 153-184.

Hall, R., Ali, J. R., and Anderson, C. D., 1995, Cenozoic motion of the Philippine Sea Plate; palaeomagnetic evidence from eastern Indonesia: Tectonics, v. 14, p. 1117-1132.

Hall, R., and Blundell, D. J., 1996, Tectonic evolution of SE Asia; introduction, in Hall, R., and Blundell, D. J., eds., Geological Society Special Publications, vol.106: London, Geological Society of London, p. 7-13.

Hannington, M. D., and Scott, S. D., 1989, Gold mineralization in volcanogenic massive sulfides; implications of data from active hydrothermal vents on the modern sea floor: Economic Geology Monographs, v. 6, p. 491-507.

Harahap, B.H., 1993, Geochemical investigation of Tertiary, magmatism rocks from West Kalimantan, Indonesia: Proceedings 22nd Annual Convention, Indonesian Association of Geologists, v. 1, p. 304-326.

Harvey, C. C., and Browne, P. R. L., 1991, Mixed-layer clay geothermometry in the Wairakei geothermal field, New Zealand: Clays and Clay Minerals, v. 39, p. 614-621.

Hay, R. L., 1968, Chert and its sodium-silicate precursors in sodium-carbonate lakes of east Africa: Contributions to Mineralogy and Petrology, v. 17, p. 255-274.

Heald, P., Foley, N. K., and Hayba, D. O., 1987, Comparative anatomy of volcanic-hosted epithermal deposits; acid-sulfate and adularia-sericite types: Economic Geology, v. 82, p. 1-26.

Hedenquist, J. W., 1986, Geothermal systems in the Taupo volcanic zone; their characteristics and relation to volcanism and mineralisation: Bulletin - Royal Society of New Zealand, v. 23, p. 134-168.

Hedenquist, J.W. 1987. Volcanic related hydrothermal systems in the circum-Pacific Basin and their potential for mineralization: Mining Geology, v. 37, p. 347-364

Hedenquist, J. W., 1990a, Mineralization of volcanic-hosted epithermal systems in the Circum Pacific, and their interpretation: Journal of the Mining and Materials Processing Institute of Japan, v. 106, p. 161-165.

Hedenquist, J. W., 1990b, The thermal and geochemical structure of the Broadlands-Ohaaki geothermal system, New Zealand: Geothermics, v. 19, p. 151-185.

Hedenquist, J. W., and Henley, R. W., 1985, Hydrothermal eruptions in the Waiotapu geothermal system, New Zealand; their origin, associated breccias, and relation to precious metal mineralization, in Sawkins, F. J., and Sillitoe, R. H., eds., Economic Geology, 80: Lancaster, Economic Geology Publishing Company, p. 1640-1668.

Hedenquist, J. W., and Roberts, P. J., 1986, Waitapu geothermal field: Monograph Series on Mineral Deposits, v. 26, p. 65-79.

Hedenquist, J. W., and White, N. C., 1995, Epithermal gold deposits; styles, characteristics and exploration, Shigen Chishitsu = Journal of the Society of Resource Geology, 45: Tokyo, Nihon Shigen Chishitsu Gakkai - Society of Resource Geologists of Japan, p. 288.

Hedenquist, J. W., Arribas, A. R., and Gonzalez-Urien, E., 2000 Exploration for epithermal gold deposits: Reviews in Economic Geology, v. 13, p. 245-277.

Henley, R. W., 1985a, Applied chemistry in the exploration and development of New Zealand geothermal systems: New Zealand Journal of Technology, v. 1, p. 207-221.

Henley, R. W., 1985b, The geothermal framework of epithermal deposits: Reviews in Economic Geology, v. 2, p. 1-24.

Henley, R. W., and Binns, R. A., 1984, Structure of active geothermal systems and implications for the origins of some hydrothermal gold and base metal ore deposits, Abstracts - Geological Society of Australia, vol.12: Sydney, Geological Society of Australia, p. 232-235.

Henley, R. W., and Brown, K. L., 1985, A practical guide to the thermodynamics of geothermal fluids and hydrothermal ore deposits: Reviews in Economic Geology, v. 2, p. 25-44.

Henley, R. W., and Ellis, A. J., 1983, Geothermal systems ancient and modern; a geochemical review: Earth-Science Reviews, v. 19, p. 1-50.

Henley, R. W., Hedenquist, J. W., and Roberts, P. J., 1986, Introduction to the geochemistry of active and fossil geothermal system: Monograph Series on Mineral Deposits, v. 26, p. 1-22.

Henley, R. W., and Plum, H., 1985, Chemistry of geothermal fluids discharged from exploration wells at Mokai/New Zealand: Zeitschrift der Deutschen Geologischen Gesellschaft, v. 136, p. 235-251.